

Dust depletion of Ca and Ti in QSO absorption line systems

C. R. Guber¹, and P. Richter^{1,2}

¹ Institut für Physik und Astronomie, Universität Potsdam, Karl-Liebknecht-Str. 24/25, 14476 Golm, Germany

² Leibniz-Institut für Astrophysik Potsdam (AIP), An der Sternwarte 16, 14482 Potsdam, Germany

Received xxx; accepted xxx

ABSTRACT

Aims. To explore the role of titanium- and calcium-dust depletion in gas in and around galaxies we systematically study Ti/Ca abundance ratios in intervening absorption-line systems at low and high redshift.

Methods. We investigate high-resolution optical spectra obtained by the UVES instrument at the *Very Large Telescope* (VLT) and spectroscopically analyze 34 absorption-line systems at $z \leq 0.5$ to measure column densities (or limits) for Ca II and Ti II. We complement our UVES data set with previously published absorption-line data on Ti/Ca for redshifts up to $z \approx 3.8$. Our absorber sample contains 110 absorbers including Damped Lyman α systems (DLAs), sub-DLAs, and Lyman-Limit systems (LLS). We compare our Ti/Ca findings with results from the Milky Way and the Magellanic Clouds and discuss the properties of Ti/Ca absorbers in the general context of quasar absorption-line systems.

Results. Our analysis indicates that there are two distinct populations of absorbers with either high or low Ti/Ca ratios with a separation at $[\text{Ti}/\text{Ca}] \approx 1$. While the calcium dust depletion in most of the absorbers appears to be severe, the titanium depletions are mild in systems with high Ti/Ca ratios. The derived trend indicates that absorbers with high Ti/Ca ratios have dust-to-gas ratios that are substantially lower than in the Milky Way. We characterize the overall nature of the absorbers by correlating Ti/Ca with other observables (e.g., metallicity, velocity-component structure) and by modeling the ionization properties of singly-ionized Ca and Ti in different environments.

Conclusions. We conclude that Ca II and Ti II bearing absorption-line systems trace predominantly neutral gas in the disks and inner halo regions of galaxies, where the abundance of Ca and Ti reflects the local metal and dust content of the gas. Our study suggests that the Ti/Ca ratio represents a useful measure for the gas-to-dust ratio and overall metallicity in intervening absorption-line systems.

Key words. quasars: absorption lines – dust, extinction – galaxies: abundances – galaxies: ISM – intergalactic medium.

1. Introduction

Systematic studies that are aiming at characterizing the chemical composition of gas and dust in the interstellar medium (ISM) and circumgalactic medium (CGM) in and around galaxies are crucial for our understanding of the formation and evolution of galaxies and their constituents.

Among the various observational strategies to measure the composition of the ISM the method of absorption spectroscopy in the ultraviolet (UV) and in the optical regime against bright background point sources stands out. It provides access to many diagnostic lines from low, intermediate, and high metal ions that can be used to explore the properties of gas in the ISM in a wide range of physical properties. In addition, from the observed deficiency of certain elements in the gas phase (commonly referred to as “depletion”) one can conclude on the composition and distribution of interstellar dust grains in the ISM and their role in the complex astrochemical balance of star-forming sites in the Universe. In our own Galaxy, UV and optical absorption-line spectroscopy can be carried out against a large number of Galactic background stars near and far, providing a detailed insight into metal abundances of heavy elements in the multi-phase ISM and dust-depletion pat-

terns (for a review see **Jenkins (2009) and Savage & Sembach (1996)**). For external galaxies beyond the Local Group, however, absorption-line spectroscopy of their ISM is limited to sightlines against extragalactic background sources, such as all sorts of active galactic nuclei (AGN; throughout the following we will use the term “QSO” for all types of AGN that can be used for absorption spectroscopy).

QSO absorption-line systems (QALS) with the highest hydrogen column densities ($\log N(\text{H I}) > 20.3$) cause strongly saturated Lyman-alpha ($\text{Ly } \alpha$) absorption in a QSO spectrum with prominent Lorentzian damping wings. Such systems therefore are called Damped-Ly α systems (DLAs). At low redshifts, DLAs most likely are associated to neutral gas in galactic discs and the inner halo regions of galaxies; they contain most of the neutral gas mass in the Universe (Prochaska et al. 2005). In sequence of further decreasing H I-column densities QALS are called subdamped Ly α -systems (Ly α absorption line saturated but dominated by the Doppler-core), and Lyman-limit systems (LLS), because their $N(\text{H I})$ is sufficient to produce continuous absorption for all absorber-restframe wavelengths smaller or equal the (redshifted) ionization edge of H I. Sub-DLAs and LLS, which contain an increasing fraction of ionized gas, are believed to characteristically arise in the extended gaseous halos of galaxies. Because QSOs are ran-

Send offprint requests to: C. R. Guber
e-mail: guber@astro.physik.uni-potsdam.de

domly distributed across the sky and because the cross section of the neutral gas regions in and around galaxies is small, QSO absorption-line studies of neutral gas in galaxies at low z beyond the Local Group require a large QSO data sample to detect DLAs, sub-DLAs, and LLS at a number that allows us to study their properties at a statistically significant level.

Next to the many lines of low, intermediate and high metal ions that can be observed in the FUV and UV for low-redshift absorbers using space-based spectrographs (such as the Cosmic Origins Spectrograph (COS) on-board the *Hubble Space Telescope* (HST) there are a few absorption lines from metal ions in near-UV and in the blue part of the optical spectrum. Of particular interest for absorption studies of neutral gas and dust in and around galaxies at low redshifts ($z \leq 0.5$) are the transitions from singly-ionized calcium (Ca II) and singly-ionized titanium (Ti II). Both, Ca II and Ti II, have near ultraviolet (UV) transitions (see Table 2), which are shifted into the visible part of the spectrum for low-redshift absorbers. This makes absorption from these lines detectable for powerful ground-based instruments (such as the Ultraviolet and Visual Echelle Spectrograph (UVES) installed at the *Very Large Telescope* (VLT)) that provide spectral data with a resolution and signal-to-noise (S/N) that typically is substantially higher than that of space-based UV spectrographs. Both elements, Ca and Ti, have comparatively high dust condensation temperatures of $T_c \gtrsim 1.5 \times 10^3 \text{ K}$ ¹. Thus, when interstellar gas cools down to temperatures below T_c , these elements are expected to belong to the elements that condense into the dust phase first. By coincidence, the ionization energy E_{ion} for Ti II nearly equals the one of neutral hydrogen. This means that both species live in the same interstellar gas phase. The ionization energy for Ca II is slightly lower than for Ti II and H I. For systems containing warm neutral gas, the true gas amount of Ca in the neutral gas phase may be larger than the one inferred from Ca II.

Previous studies of Ti II and Ca II in the Milky Way, in the Small & Large Magellanic Cloud, and in intervening QALS at high redshift by Welty & Crowther (2010) indicate that in low-metallicity systems the Ti/Ca ratio is substantially raised compared to the Milky Way (Welty & Crowther 2010). This trend can be explained by the lower metal and dust content and different gas/dust properties in such systems. In this scenario, the increase of Ti/Ca ratio with *decreasing* metallicity/dust abundance then reflects the distinct dust depletion properties of the elements Ti and Ca: while Ca appears to be severely depleted even in low-metallicity gas, strong Ti depletion appears to be relevant only for high-metallicity environments (see Welty & Crowther (2010)). The dust-to-gas ratio and the ionizing radiation field (that strongly influences the abundance of Ca II in predominantly neutral gas) can, however, vary substantially within gaseous structures in and around a galaxies (see Richter et al. (2011)). For instance, the dust-depletion patterns found in diffuse clouds in the Milky Way halo are remarkably distinct from those found in the dense regions in the Milky Way disk **with a more or less continuous transition between them** (see Jenkins (2009) and Savage & Sembach (1996)). A systematic study of Ti II and

Ca II in QALS at low and high redshift and their relation to galaxies therefore not only holds the prospect of increasing our understanding of dust abundances and depletion patterns in the interstellar media of gas-rich galaxies. It also provides important information on the distribution and properties of neutral gas structures beyond the stellar disks in galaxies, such as in high-velocity clouds and in circumgalactic tidal gas streams (e.g., Fox et al. 2013, 2014; Richter et al. 2014).

In this study, we examine 34 low- z ($z \leq 0.5$) Ca II-selected QALS observed with VLT/UVES to study their Ti II abundance and the Ti II/Ca II ratios and investigate the gas and dust properties of the absorbers. We complement our data with literature information on Ti II and Ca II in the Milky Way, the Magellanic Clouds, and high-redshift absorbers. We further collect information about the column densities of H I and Zn II in the absorbing systems, explore the association of absorbers with galaxies, study the ionization properties of Ti II/Ca II gas, and correlate the Ti II/Ca II ratios with other relevant quantities.

The paper is organized as follows. In Sect. 2 we shortly describe the observations, the spectral data and the analyzing methods. In Sect. 3 we discuss the absorption properties of the Ca II/Ti II systems and investigate important parameter correlations. A comparison between the absorber properties in our QSO sample and other, local Ca II/Ti II absorbing environments (Milky Way, Magellanic Clouds) is provided in Sect. 4. In Sect. 5 we model the ionization conditions in Ca II/Ti II absorbers. Finally, a summary of our study is given in Sect. 6.

2. Observations, data, and analyzing methods

2.1. UVES data

For our study we examined 34 high-resolution² ESO UVES/VLT spectra of QSOs (with emission redshifts predominantly higher than 0.5) for intervening Ca II and Ti II absorption at redshifts $z \leq 0.5$. **A example spectrum is shown in Fig. 1.** Information about the examined QSO is provided in Table 2.

The study continues and extends our previous survey of intervening Ca II absorbers at low redshift presented in Richter et al. (2011). The UVES data are publically available in the ESO archive. Here we use data that have been extracted and pre-reduced as part of the SQUAD project (PI: M. Murphy) using a modified version of the UVES reduction pipeline. For more details on the data reduction and the procedure of identifying intervening Ca II absorbers in the spectra see Richter et al. (2011).

For the (independent) analysis of the absorbers we used the the ESO/MIDAS software executing the following steps. First, we used the absorber redshifts given in Richter et al. (2011) to create restframe-velocity plots of all lines of interest (i.e., the lines from Ca II and Ti II, but also lines from Na I and Mg II; see Table 1). We then rejected all blended absorption lines (i.e., lines that exhibit an unexpected absorption behavior according to the known different oscillator strengths of the transitions). We re-normalized the spectra in the vicinity of every line of interest using low-order polynomials, determined the local signal to noise ratio $(S/N)_{\text{vb}}$ per velocity bin Δv_{pixel} , and

² $R := \lambda/\Delta\lambda \geq 45.000$

¹ T_c for a specific element is the temperature below which 50 % of the total amount is condensed into the dust phase (Wasson 1995).

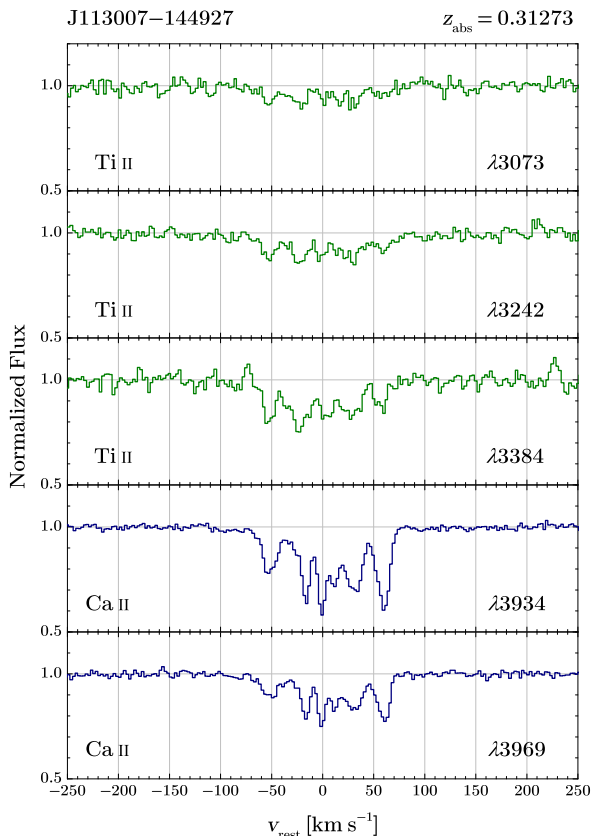


Fig. 1. Example for velocity profiles of Ti II and Ca II in our UVES spectra, here for the absorber at $z_{\text{abs}} = 0.31273$ towards J113007–14492. In this system, a multi-component structure is evident in both Ca II as well as in Ti II.

finally determined the observed equivalent width by a direct pixel integration. **Within the sample the S/N per resolution element varies between 9 and 540.** All the systems examined in this study show unsaturated Ca II and Ti II absorption in their respective transitions. Therefore, we use the apparent-optical depth (AOD) method (Savage & Sembach 1996) to derive column densities for the various ions from the various absorption lines. For each ion, we calculated the error-weighted mean column density from the values derived for each individual line

$$\bar{N} = \frac{\sum_i p_i N_i}{\sum_i p_i}; \quad p_i = \frac{1}{\Delta N_i^2}. \quad (1)$$

We computed the uncertainty of the error-weighted mean value for the case of no relevant systematic errors (“internal consistency”),

$$\Delta \bar{N} = \sqrt{\frac{1}{\sum_i p_i}} \quad (2)$$

as well as the standard deviation of the weighted mean value (“external consistency”)

$$\Delta \bar{N} = \sqrt{\frac{\sum_i p_i (N_i - \bar{N})^2}{(n-1) \sum_i p_i}} \quad (3)$$

Table 1. Vacuum wavelengths and oscillator strengths used in this paper. Values are taken from Morton (2003).

Ion & Transition	λ_{vac} [Å]	f
Ti II $\lambda 3073$	3073.863	0.121
Ti II $\lambda 3242$	3242.918	0.232
Ti II $\lambda 3384$	3384.730	0.358
Ca II $\lambda 3934$	3934.7750	0.6267
Ca II $\lambda 3969$	3969.5901	0.3116

and rejected the smaller one of both error values. In case that at the wavelength of the (unblended) absorption line with the strongest oscillator strength no absorption feature is visible the determination of a 4σ upper limit (UL) for the column density is possible using the signal to noise ratio per resolution element (e.g., Tumlinson et al. (2002), Richter et al. (2001)) via the relation

$$N_{\text{UL}} = 1.13 \times 10^{20} \text{ cm}^{-2} \frac{4}{R (S/N)_{\text{re}} f (\lambda_0/\text{Å})}, \quad (4)$$

where $R = \lambda/\Delta\lambda$ is the spectral resolution, $(S/N)_{\text{re}}$ the signal-to noise ratio per resolution element, f the oscillator strength, and λ_0 the restframe wavelength of the transition.

2.2. Supplementary data

We supplement our own measurements with literature values of Ca II and/or Ti II column densities in 76 QALS at predominantly high ($z > 1$) redshifts, as compiled by Welty & Crowther (2010). We also searched in the astrophysical database SIMBAD for galaxies within 2 Mpc that could be associated with the absorbers and derived corresponding impact parameters.

To relate the observed Ti/Ca ratios in intervening metal absorbers to the overall metallicity of the absorbing gas, information on other observable metal ions are useful. Among the various weakly-ionized metal ions, the element zinc (Zn) is particularly important for this purpose. Compared with Ti and Ca, the depletion of Zn under normal interstellar conditions is expected to be very small and thus can be neglected (Savage & Sembach (1996); Timmes, Lauroesch & Truran (1995)), **although (Jenkins 2009) found evidence for mild Zn-depletions in dense interstellar conditions.** With an ionization energy larger than that of H I singly-ionized zinc (Zn II) is assumed to be the dominant ionization state in neutral interstellar gas. Therefore, the observed Zn II/H I ratio serves as a robust measure for the absolute Zn abundance and the overall metallicity of the gas. For our study we therefore have collected all available information on the Zn abundances in the sample of Ti/Ca absorption systems from the literature.

Throughout the paper we use a Λ CDM cosmology with $H_0 = 67.3 \text{ km s}^{-1} \text{ Mpc}^{-1}$, $\Omega_{\text{M}} = 0.315$ and $\Omega_{\text{V}} = 0.685$ (Planck Collaboration 2014)) and solar reference abundances from Asplund et al. (2009). The results from our line fitting and literature search are presented in Tables A1–A4 in the Appendix.

In this paper all column densities N are given in cm^{-2} , all 3-dimensional particle densities in cm^{-3} .

Table 2. Quasar data (obtained from SIMBAD) for sightlines with QALS for which we derived Ti II column densities from VLT/UVES. Coordinates in ICRS(epJ2000).

Quasar name	Alternative names	α_{2000} [h min s]	δ_{2000} [$^{\circ}$ ' '']	z_{em}
J000344–232355	QSO J0003–2323, HE 0001–2340	00 03 44.92	–23 23 54.8	2.280
J005102–252846	LBQS 0048–2545, QSO B0048–2545	00 51 02.3	–25 28 48	2.082
J012517–001828	QSO B0122–005, PKS 0122–005	01 25 17.1498	–00 18 28.878	2.276
J014125–092843	QSO J0141–0928, PKS 0139–09, QSO B1038–097	01 41 25.83179	–09 28 43.6791	1.034
J030844–295702	no quasar found in SIMBAD	–	–	–
J042707–130253	QSO J0427–1302, PKS 0424–131, QSO B0424–131	04 27 07.3003	–13 02 53.644	2.166
J044117–431343	QSO J0441–4313, QSO B0439–433, HE 0439–4319, PKS 0439–433	04 41 17.32	–43 13 45.4	0.594
J045608–215909	QSO J0456–2159, HE 0454–2203, PKS 0454–22	04 56 08.9272	–21 59 09.543	0.534
J050112–015914	4C –02.19, QSO B0458–0203, PKS 0458–020	05 01 12.80988	–01 59 14.2561	2.286
J051707–441055	QSO B0515–4414, 4E 0515–4414	05 17 07.63	–44 10 55.5	1.713
J055158–211949	QSO B0549–213, QSO J0551–2199	05 51 58.3	–21 19 50	2.245
J094253–110426	QSO B0940–1050, QSO J0942–1104, HE 0940–1050	09 42 53.49	–11 04 25.9	3.054
J095456+174331	QSO B0952+179, PKS 0952+179	09 54 56.82362	+17 43 31.222	1.475
J102837–010027	LBQS 1026–0045B, QSO B1026–0045B	10 28 37.0163	–01 00 27.555	1.532
J104733+052454	QSO B1044+056	10 47 33.1551	+05 24 54.882	1.334
J110325–264515	QSO B1101–26, PG 1101–264	11 03 25.31	–26 45 15.875	2.145
J113007–144927	QSO J1130–1449, PKS 1127–145, QSO B1127–14	11 30 07.0473	–14 49 27.424	1.189
J121140+103002	LBQS 1209+1046, QSO B1209+1046	12 11 40.5903	+10 30 02.026	2.193
J121509+330955	QSO J1215+3309, Ton 1480, QSO B1212+3326	12 15 09.2208	+33 09 55.233	0.615
J123200–022404	4C –02.55, QSO B1229–021, PKS 1229–021	12 32 00.160	–02 24 04.794	1.043
J124646–254749	QSO J1246–2547, PKS 1244–255, QSO B1244–255	12 46 46.8006	–25 47 49.371	0.638
J133007–205616	QSO B1327–2040, PKS 1327–206	13 30 07.7	–22 56 16.5	1.165
J142249–272756	QSO B1420–272, PKS 1419–272	14 22 49.2317	–27 27 56.857	0.985
J142253–000149	QSO J1422–001, QSO B1420–0011	14 22 53.3157	–00 01 49.077	1.083
J144653+011356	LBQS 1444+0126, QSO B1444+0126	14 46 53.0	+01 13 55	2.210
J162439+234512	4C 23.43, QSO B1622+238, PKS 1622+238	16 24 39.0847	+23 45 12.183	0.927
J215501+092224	QSO J2155–0922, PHL 1811, QSO B2152–0936	21 55 01.5152	+09 22 24.688	0.192
J220743–534633	QSO B2204–54, PKS 2204–540	22 07 43.7420	–53 46 33.826	1.206
J224752–123719	QSO B2245–1282, PKS 2245–128	22 47 52.6411	–12 37 19.721	1.892
J231359–370446	QSO B2311–373, PKS 2311–373	23 13 59.7	–37 04 46	2.476
J232820+002238	QSO J2328+0022, QSO B2325+0006	23 28 20.3797	+00 22 38.262	1.302
J235731–112539	QSO B2354–117, PKS 2354–117	23 57 31.1976	–11 25 39.176	0.960

3. Absorber properties and classification

To characterize the absorption properties of the systems in our sample we start our analysis by looking for correlations between the measured column densities of Ca II, Ti II, H I, and Zn II. Our analysis strategy is summarized as follows.

First, we divide our absorbers in different sub-samples, depending on whether Ti II is detected or not. We then explore Ti/Ca-ratios in our absorption systems and compare them with previous measurements in the Milky Way and in the Magellanic Clouds (Sect. 3.1). For systems for which H I information is available we investigate the relation between Ca II, Ti II and the total neutral gas column density (Sect. 3.2). In Sect. 3.3 we explore the number density of intervening Ti II-absorbers.

From our 34 absorption-line systems, 27 exhibit absorption in Ca II, but only 5 show significant absorption in Ti II. For all systems we have measured equivalent widths (equivalent-width limits) and column densities (column-density limits) of Ca II and/or Ti II following the procedure outlined in Sect. 2. Because of the inhomogeneity of the absorber sample we divide our systems into different samples according to the detection/non-detection of the different metal ions:

1. Sample A: Ca II systems with known $N(\text{Ti II})$,
2. Sample B: Ca II systems with upper limits for $N(\text{Ti II})$,

Information about Samples A & B are compiled in Table A.1 (Appendix). This table also contains all Ca II systems taken from Welty & Crowther (2010) that can be classified as sample A or B. Table A.2 in the Appendix gives information about all Ti II systems from Welty & Crowther (2010) without any information about Ca II-column densities. Finally, Table A.3 (Appendix) lists all the systems of our data sample and from Welty & Crowther (2010) with only upper limits for the column densities of both, Ca II and Ti II and Ca II systems without any information about Ti II.

The absorbers considered in this study span a huge redshift range between $z_{\text{abs}} = 0.003$ and 3.774. The redshift-dependence of the observed absorber properties will be discussed in Sect. 4.

3.1. Observed Ti/Ca ratios

In Fig. 2 we plot $\log N(\text{Ti II})$ vs. $\log N(\text{Ca II})$ for the absorbers in samples A and B.

For comparison, the Magellanic Cloud absorbers and high-redshift systems presented by Welty & Crowther

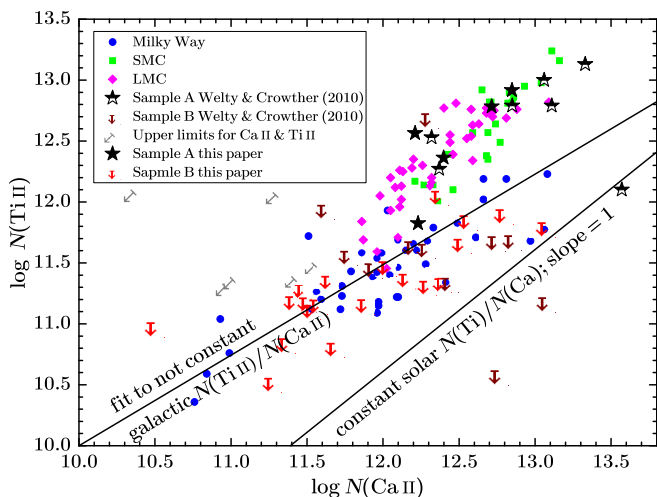


Fig. 2. $\log[N(\text{Ti II})]$ vs. $\log[N(\text{Ca II})]$ for QALS for which Ca II and Ti II column densities (sample A) or upper limits therefore (sample B) are available. ALS in the Magellanic Clouds as well as in the Milky Way are shown, too. With the one exception showing a solar like Ti/Ca-ratio all the sample A systems have supersolar Ti/Ca-ratios. Systems with constant, solar Ti/Ca-ratio would lay on the black line with slope 1. The other black line represents the linear fit of the Galactic ALS already published by Welty & Crowther (2010). Its slope < 1 indicates decreasing Ti/Ca-ratio with increasing Ca II-column density.

(2010) are also shown. In addition, we indicate the solar Ti/Ca ratio and the measured trend for $\log N(\text{Ti II})$ vs. $\log N(\text{Ca II})$ in the Milky Way ISM with black solid lines.

For the Ca II systems with known values for $N(\text{Ti II})$ (sample A) we find that all except one of the systems have Ti II/Ca II ratios that lie clearly above the solar Ti/Ca ratio and also above the relation observed in the Milky Way ISM. Comparison with the data points from Welty & Crowther (2010; data points) instead indicates that the systems from sample A are distributed in the same region in this plot where also the SMC and LMC absorbers are found.

For the Ca II systems without known Ti II column densities (sample B) the interpretation of the observed distribution of data points (=limits) is less straight-forward. All the examined systems were studied with high resolution spectra that have (in most cases) comparable signal-to-noise ratios. Therefore, one can expect to obtain similar upper limits for $N(\text{Ti II})$ for most of the absorbers, independent of $N(\text{Ca II})$. This indeed is the case: 75% of the class 2 systems have upper limits (ul) of $\log N(\text{Ti II})_{\text{ul}} \in [11 - 12]$. Systems from sample B that have $\log N(\text{Ca II}) < 12$ do not provide useful information because their values for $N(\text{Ti II})_{\text{ul}}$ are so high, that they could have Ti/Ca ratios that are either lower, equal or larger than the solar reference value.

In contrast, for the systems in sample B that have $\log N(\text{Ca II}) > 12$ (especially the ones with $\log N(\text{Ca II}) > 12.5$) we can conclude that they exhibit Ti/Ca ratios that are comparable to or even lower than the solar one (see Fig. 2). For the systems with $\log N(\text{Ca II}) \gtrsim 12$, the lack of absorbers showing Ti/Ca ratios between solar and supersolar solar values with $[\text{Ti}/\text{Ca}] \gtrsim 1$ indicates that Ca II absorbers can be subdivided into two classes:

1. Class 1: systems with $[\text{Ti}/\text{Ca}] \gtrsim 1$, and
2. Class 2: systems with $[\text{Ti}/\text{Ca}] \lesssim 0$.

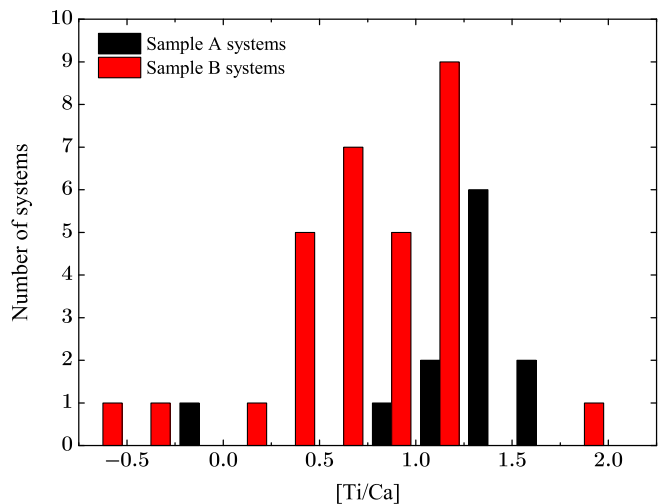


Fig. 3. Histogram comparing the Ti/Ca-ratios of sample A & B systems. Except the one sample A system with $[\text{Ti}/\text{Ca}] = -0.08$ all sample A systems are high Ti/Ca systems with $[\text{Ti}/\text{Ca}] \gtrsim 1$.

In Fig. 3 we show a histogram for absorbers from samples A and B that displays the number of corresponding systems in specific intervals for $[\text{Ti}/\text{Ca}]$. Except the one system from sample A that has $[\text{Ti}/\text{Ca}] = -0.08$, all sample A absorbers have $[\text{Ti}/\text{Ca}]$ ratios according to the above defined class 1 ($[\text{Ti}/\text{Ca}] \gtrsim 1$). Sample-A absorbers have a mean $[\text{Ti}/\text{Ca}]$ ratio of $\langle [\text{Ti}/\text{Ca}] \rangle = 1.34$, where the uncertainty for the individual measurement is 0.21 dex and an uncertainty for the average value is 0.07 dex. **Note that the individual values for sample B systems are only upper limits, so that the true mean value of this group is even lower than the mean value of upper limits** $\langle [\text{Ti}/\text{Ca}]_{\text{ul}} \rangle = 0.8$. **Although within sample B there might be a few systems with high Ti/Ca ratios belonging to Class 1, most of them exhibit Ti/Ca-ratio limits that are more comparable to or even lower than the solar value (\rightarrow class 2).** Except the one outlier sample A system with $[\text{Ti}/\text{Ca}] \approx 0$, there is a one-to-one correspondence between sample A absorbers and class 1 systems.

In the following sections, we will further investigate whether the separation into two different absorber classes is a result of the different dust (depletion) properties in the gas, or is caused by ionization effects, or by a combination of these two aspects.

3.2. Associated H I absorption

Only for a small sub-sample of the Ca II/Ti II systems in our sample literature values for the H I column densities (from their Ly α absorption and/or 21 cm emission) are available (see Tables A.1 & A.3 for corresponding references).

In Fig. 4 we show the H I column density dependence for $N(\text{Ca II})$ (left panel) and $N(\text{Ti II})$ (right panel) for absorbers in samples A and B. There are a number of interesting trends visible that can be summarized as follows:

1. For both, Ca II and Ti II systems from sample A the column densities increase with increasing $N(\text{H I})$. The relation for Ti II is relatively tight, while for Ca II there is considerable scatter. From a fit of the data points we

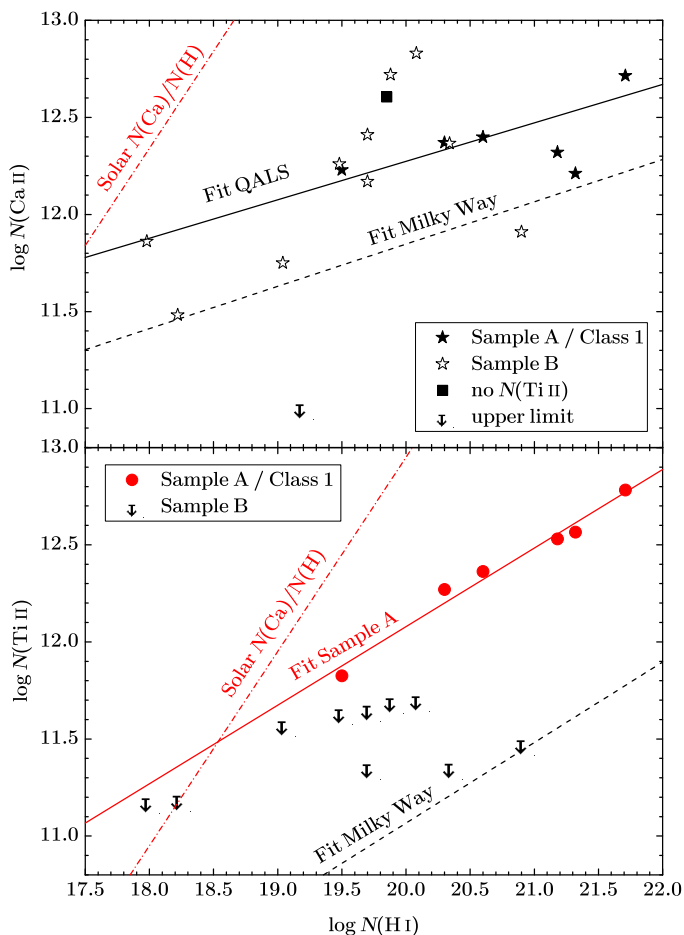


Fig. 4. $\log N(\text{Ca II})$ and $\log N(\text{Ti II})$ vs. $\log N(\text{H I})$. Every sample A system in the plots above is also a class 1 system. Filled box in the Ca II-plot: the one Ca II system without any Ti II-information; the arrow represents the one Ca II system with only upper limits both for Ca II & Ti II. In case Ca II or Ti II is the dominant ionization state, systems with solar Ca/H (Ti/H) ratio would lay on the line-dotted lines with slope 1. The dashed lines represent linear fits of galactic values (Ca II from Wakker & Mathis (2000), Ti II from Welty & Crowther (2010)).

derive a slope of $A = 0.198 \pm 0.077$ (offset $n = 8.3 \pm 1.6$) for the relation $\log N(\text{Ca II}) = A \log N(\text{H I}) + n$ and $B = 0.404 \pm 0.031$ (offset $m = 4.00 \pm 0.65$) for the relation $\log N(\text{Ti II}) = B \log N(\text{H I}) + m$.

2. For a given $N(\text{H I})$ the column densities of Ca II and Ti II (sample A) are substantially larger than typically observed in the Milky Way. The corresponding offsets are $\sim +0.4$ dex for Ca II and $\sim +0.9$ dex for Ti II (see Richter et al. (2011) & Welty & Crowther (2010)).
3. The slopes of the above given fits for both QALS and Milky Way clouds are much smaller than unity. This trend indicates decreasing Ca/H and Ti/H ratios in the gas phase for increasing $N(\text{H I})$, a typical signature of column-density dependent dust depletion. In addition, the different slopes of Ca II and Ti II suggest that Ti/Ca in the gas phase is increasing for increasing $N(\text{H I})$, a signature for non-uniform differential depletion properties of these two elements; this aspect will be further investigated below.
4. The Ti II upper limits of the systems in sample B (presumably class 2 absorbers) are in contradiction to the

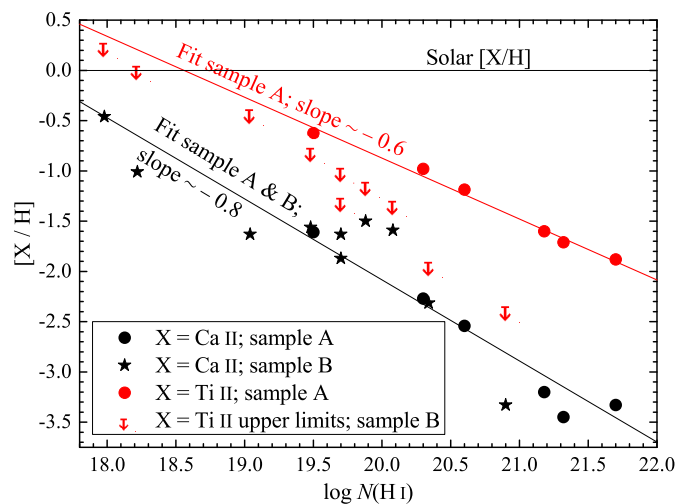


Fig. 5. $[\text{Ca}/\text{H}]$ and $[\text{Ti}/\text{H}]$ vs. $\log N(\text{H I})$. In case of Ti II the solid line represents the linear fit of the sample A systems, which in this case are all class 1 systems, too. In case of Ca II the solid line represents the linear fit of all systems with known $N(\text{Ca II})$. Systems with solar Ca/H or Ti/H ratios would lay on the horizontal solid line with $[\text{X}/\text{H}] = 0$.

Ti II column densities in sample A (class 1; Fig. 4). All the absorbers in sample B have $\log[N(\text{Ti II})] < 11.8$, even for comparatively high $N(\text{H I})$. This trend supports our previously outlined scenario in which the absorbers can be separated into two sub-classes: absorbers with comparatively high Ti/Ca ratios ($[\text{Ti}/\text{Ca}] \gtrsim 1$) (class 1), that also have high Ti II/H I ratios, and absorbers with low Ti/Ca ratios ($[\text{Ti}/\text{Ca}] \approx 0$) (class 2), that also have low Ti II/H I ratios.

As mentioned above, the observed trends for Ca II/H I and Ti II/H I in our survey indicate non-uniform differential dust depletions for Ca and Ti in the absorbing gas environments. To further investigate this aspect in Fig. 5 we show the ratios $[\text{Ca}/\text{H}]$ or $[\text{Ti}/\text{H}]$ as function of $\log N(\text{H I})$. Both the $N(\text{H I})$ -dependency of $[\text{Ca}/\text{H}]$ (for all the Ca II absorbers) and $[\text{Ti}/\text{H}]$ (only for sample A/class 1) can well be described by (linear) relations. The scatter around the fitted relations is more severe for $[\text{Ca}/\text{H}]$ than for $[\text{Ti}/\text{H}]$ (class 1), as expected from the trend seen in Fig. 4 (see also Richter et al. (2011), their Fig. 9). In addition, the slope for $[\text{Ca}/\text{H}]$ (-0.806 ± 0.075) is slightly steeper than the one for $[\text{Ti}/\text{H}]$ (-0.599 ± 0.032). For the sample A/class 1 systems this again indicates that the Ti/Ca ratios *increase* with increasing $N(\text{H I})$.

If we plot $[\text{Ti}/\text{Ca}]$ directly against $\log N(\text{H I})$ (Fig. 6), we see this trend directly for sample A/class 1 systems, where the $[\text{Ti}/\text{Ca}]$ -H I relation can be well fitted linearly with a slope of $+0.282 \pm 0.083$. **Systems in sample B show a different behavior than sample A/class 1 systems and do not all lay on or above the trend for class 1 systems.**

3.3. Number density of intervening Ti II absorbers

Only five out of the 34 originally selected Ca II absorbers at $z < 0.5$ from the sample of 270 (304) QSOs presented in (Richter et al. 2011) show associated Ti II absorption (see Table A.1), suggesting that intervening Ti II absorbers

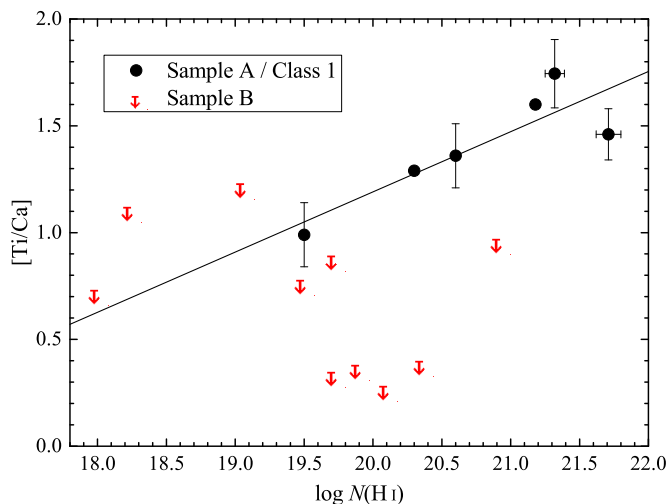


Fig. 6. $[\text{Ti}/\text{Ca}]$ vs. $\log N(\text{H I})$ for sample A & B systems. All sample A systems in this plot are also class 1 systems. The black line represents the non weighted linear fit of the sample A data. The distribution of the class 2 systems can't be described by this fit.

in the local Universe are very rare. This is, however, not surprising at all in view of the substantially lower cosmic abundance of Ti compared to Ca ($\log (\text{Ti}/\text{H})_{\odot} = -7.05$ vs. $\log (\text{Ca}/\text{H})_{\odot} = -5.66$; Asplund et al. (2009)) and the relatively small oscillator strengths of the available Ti II transitions compared to the Ca II H&K lines (Table 1). Thus, for a typical detection limit of $\log N(\text{Ti II}) = 12.0$ in UVES data and a typical metallicity of ≤ 0.1 solar, one requires a neutral gas column as large as $\log N(\text{H I}) > 20$, even if the dust depletion of Ti is zero. Ti II-absorbing systems that do not show significant Ca II absorption are not expected to exist (except Ca II is blended by other lines or is located outside the observable wavelength range). The detection of Ti II in an intervening absorber thus depends on three parameters: the total gas column density, the overall metallicity, and the depletion of Ti into dust grains.

All five Ti II absorbers in the UVES data sample analyzed in this study represent class 1 absorbers with high Ti II/Ca II ratios (Table A.1) spanning a column density range of $\log N(\text{Ti II}) = 11.8 - 13.0$. Based on the distribution of S/N in UVES data set (described in detail by Richter et al. (2011)) and using equation 1 together with atomic data of the available Ti II transitions (Table 1) we calculate that all the 270 selected UVES spectra from the Ca II survey of (Richter et al. 2011) are sensitive to Ti II column densities of $\log N(\text{Ti II}) \geq 12.0$, where the total redshift path to detect Ca II/Ti II systems in these spectra is $\Delta z = 89.15$. Four out of the five Ti II absorbers have Ti II column densities above this limit, so that we derive a number density of intervening Ti II absorbers with $\log N(\text{Ti II}) \geq 12.0$ at $z < 0.5$ of $dN/dz = 4/270 = 0.045 \pm 0.023$.

Because of a potential selection bias in the UVES absorber sample (see the detailed discussion in Richter et al. (2011)) this value might be overestimated by up to 40 per cent, so that the true number density might be even lower. If we correct for this bias and reduce the number density by 40 per cent we obtain $dN/dz = 0.027 \pm 0.017$.

This value now can be compared to the number density of sub-DLAs and DLAs absorbers at low redshift. Three of the low-redshift absorbers in our UVES sample are high-column density systems with $\log N(\text{H I}) > 20.1$ (while for the fourth system no information on $\log N(\text{H I})$ is available). All but one of the high-redshift Ti II absorbers with $\log N(\text{Ti II}) \geq 12.0$ compiled by Welty & Crowther (2010) have $\log N(\text{H I}) > 20.1$, suggesting that Ti II absorption at this column-density level typically arises in DLAs and high-column density sub-DLAs (see Table A2 in the Appendix).

From the 21 cm H I mass function in the local Universe Zwaan et al. (2005) derives $dN/dz = 0.060$ for absorbers with $\log N(\text{H I}) > 20.1$, a number density that is 2.2 times higher than the estimated $dN/dz(\text{Ti II}) = 0.027$ at low redshift. From this we conclude that only ~ 45 per cent of high-column density sub-DLAs and DLAs exhibit Ti II absorption with $\log N(\text{Ti II}) \geq 12.0$. On the other hand, for more than half (~ 55 per cent) of such absorbers the combined effect of low metallicity and dust depletion leads to a reduction of Ti in the gas phase in these systems by at least 1 dex when compared to the solar Ti reference abundance ($20.10 - 12.00 - 7.05 = 1.05$; see above).

In Sect. 4.2.2 we will further explore the degeneracy between metallicity and dust depletion effects in these absorption systems by considering absorption-line measurements of interstellar zinc.

3.4. Preliminary interpretation of observed trends

The various trends presented in the previous sub-sections demonstrate that the Ca/Ti absorbers in our sample trace a broad range of gaseous environments in the inner and outer regions of galaxies and in the circumgalactic environment. The sub-division on the absorbers into two different classes (class 1 and class 2) is justified in view of the different behavior of these two absorber classes concerning the observed Ca II/Ti II and Ti II/H I ratios (see previous section). Since Ti II and H I have identical ionization potentials, the different trends for Ti II/H I for the two classes must originate in different dust-depletion properties and/or Ti abundances in the two absorber classes. If dust is (primarily) responsible for the observed trends, then class-1 absorbers trace optically thick gaseous regions in and around galaxies that have substantially less dust depletion of Ti than class-2 systems. The apparent lack of dust depletion in class-1 systems may be related to a different size or composition of dust grains in such environments (see, e.g., Draine (2003)) or simply caused by a lower dust-to-gas ratio. From the discussion in the previous section on the observed number density of Ti II-absorbing systems at low redshift follows that possibly half of the high-column density sub-DLAs and DLAs with $\log N(\text{H I}) > 20.1$ may belong to this category of absorbers.

Because of the steeper decline of $[\text{Ca}/\text{H}]$ with H I the effect of dust depletion in the absorption systems is more severe for Ca, a trend that is well known for Milky Way gas (Savage & Sembach 1996). However, also photo-ionization affects the gas-phase abundance of singly-ionized Ca in interstellar gas, owing to the fact that the ionization potential of Ca II is smaller than that of H I. For the interpretation of the observed Ca/Ti ratios in the absorbers with respect to the nature and origin of the gas (for instance, disk gas vs. halo gas), a detailed photoionization modeling therefore is required. Such a modeling will be presented in Sect. 5.

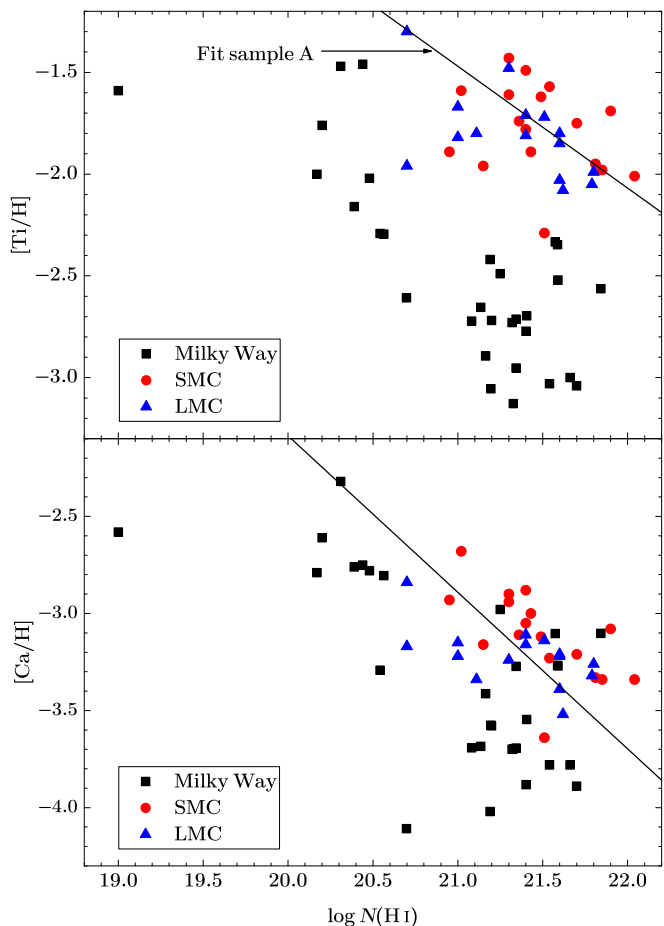


Fig. 7. $[\text{Ti}/\text{H}]$ and $[\text{Ca}/\text{H}]$ vs. $\log N(\text{H I})$ of absorption line systems in the Milky Way and the Small & Large Magellanic Clouds (SMC and LMC, respectively). In case of $[\text{Ti}/\text{H}]$ the solid line represents the linear fit of the sample A systems, which in this case are class 1 systems, too. In case of $[\text{Ca}/\text{H}]$ the solid line represents the linear fit of all the QALS for which Ca II as well as H I column densities are available.

4. Comparison with Ca/Ti/H observations in other environments

4.1. Milky Way and the Magellanic Clouds

In the Milky Way ISM, the measured Ca II/Ti II ratios imply $[\text{Ti}/\text{Ca}]$ ratios that are typically far below the ones seen in QALS, with a mean value of about $\langle [\text{Ti}/\text{Ca}] \rangle = -0.9$ (e.g., Hunter et al. (2006)). The absolute depletion of Ti in the Milky Way ISM varies between ~ 1.3 dex for warm, diffuse gas and ~ 3.0 for cold, dense gas, if the ζ Ophiuchi cloud is taken as reference (see Savage & Sembach 1996). In the Magellanic Clouds, the typical depletion of Ti into dust grains appears to be significantly smaller than in the Milky Way (see Welty & Crowther (2010) and references therein), indicating a lower dust-to-gas ratio and/or different grain properties.

When plotting $\log N(\text{Ti II})$ vs. $\log N(\text{Ca II})$ in our sample, class-1 absorbers follow the trend seen in the Magellanic Clouds, while the data points (=limits) for class-2 systems are in accordance with the trend seen in the Milky Way (see Fig. 2). To further compare the observed trends in QALS with those in the Milky Way (MW) and the Magellanic

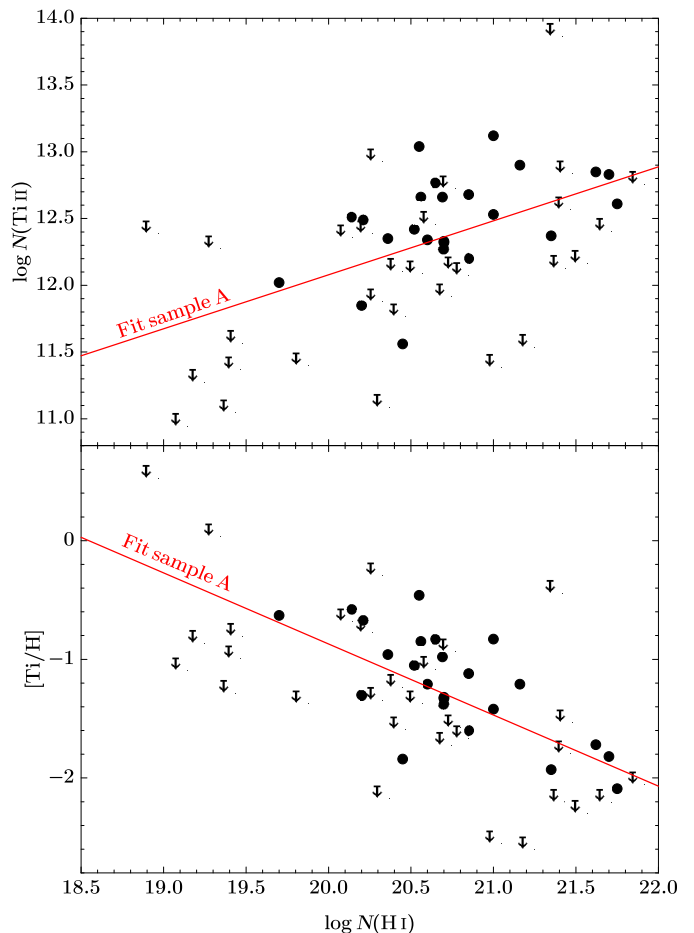


Fig. 8. $\log N(\text{Ti II})$ and $[\text{Ti}/\text{H}]$ vs. $\log N(\text{H I})$ for Ti II systems without any information about the Ca-content from Table A.2. The solid red lines represent the fits of the sample A/ class 1 systems.

Clouds (MCs) in Fig. 7 we plot the abundance ratios $[\text{Ti}/\text{H}]$ (upper panel) and $[\text{Ca}/\text{H}]$ (lower panel) as a function of the neutral gas column density for the MW/MCs from Welty & Crowther (2010) together with the fitted trend seen for the intervening absorbers in sample A (Fig. 4). Also here it is evident that the QALS in sample A are much closer to the SMC data points than to the data points in the Milky Way, indicating that the depletion of Ti and Ca into dust grains is substantially smaller in QSALS than in the Milky Way on a level that is comparable to the one in the SMC. This behavior most likely reflects a lower (average) dust-to-gas ratio in these systems and/or a larger fraction (cross section) of warm, diffuse gas in which the dust depletion is expected to be generally smaller than in cold, dense gas (see above).

If most QALS typically have depletion properties similar to the SMC rather than similar to the Milky Way, this aspect needs to be considered in the interpretation of the observed abundances of dust-depleted elements in QALS. In fact, as pointed out by Welty & Crowther (2010), comparing the abundance trends in intervening absorbers with the depletion pattern of heavy elements in the Milky Way ISM may lead to inappropriate conclusions about the dust content and enrichment history of these systems.

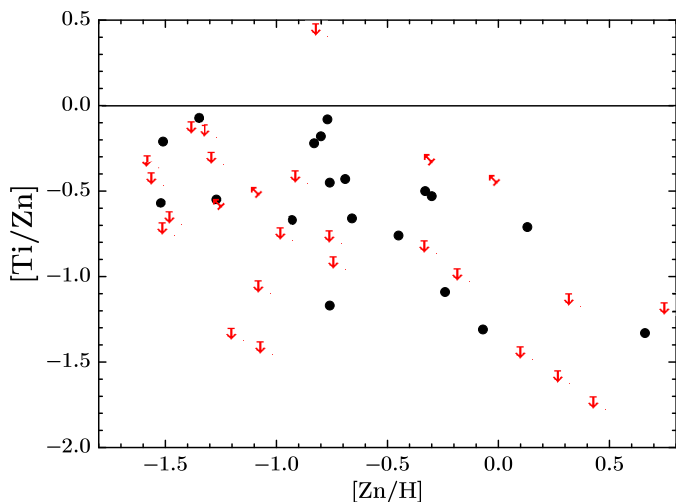


Fig. 9. $[\text{Ti}/\text{Zn}]$ vs. $[\text{Zn}/\text{H}]$. In contrast to Ti, the portion of Zn, which is depleted into dust grains can be expected to be comparatively small. Therefore $[\text{Ti}/\text{Zn}]$ can be treated as a good indicator of dust depletion. Also because of this $[\text{Zn}/\text{H}]$ is a good indicator for the metallicity of the observed system. This plot shows that on average dust depletion is more severe in systems with higher metallicity.

4.2. Other intervening absorption-line systems

Systems for which no Ca column densities or upper limits are available obviously cannot be used to study Ti/Ca ratios in intervening absorbers. However, these systems can be used to test the above-stated hypothesis that the Ti depletion is more severe for increasing metallicity of the gas.

4.2.1. Ti-absorbers without Ca information

In Fig. 8 we show the column densities for Ti II over H I (upper panel) and $[\text{Ti}/\text{H}]$ over H I (lower panel) for the 51 predominantly high-redshift absorbers from the list of Welty & Crowther (2010), for which there is no information on the Ca II column density. These systems are listed in Table A.2 in the Appendix. Although there is remarkable scatter in the plots, these high-redshift systems predominantly follow the same trends for Ti II over H I as the Ca II-selected systems from sample A/class 1, as presented in Sect. 3.2 (Fig. 8, solid red lines). From this we conclude that the initial Ca II selection criterion for the low-redshift absorbers in our UVES sample apparently does not introduce a bias into the distribution of Ti II/H I ratios in our absorber sample.

4.2.2. General metallicity dependency of dust depletion

To further investigate the relation between dust-depletion of Ca and Ti and the overall metal abundance in the absorbers we consider supplementary information on singly-ionized Zn (see Sect. 2). The Zn II column densities are listed in Table A.2 in the Appendix.

In Fig. 9 we plot the $[\text{Ti}/\text{Zn}]$ ratio as a function of the Zn abundance $[\text{Zn}/\text{H}]$ (i.e., the metallicity) of the absorbers. The trend seen in this figure indicates that the depletion of Ti increases for increasing metallicity, possibly because of an increase of the dust-to-gas ratio for increasing metallicity. The scatter is substantial but not surprising, because

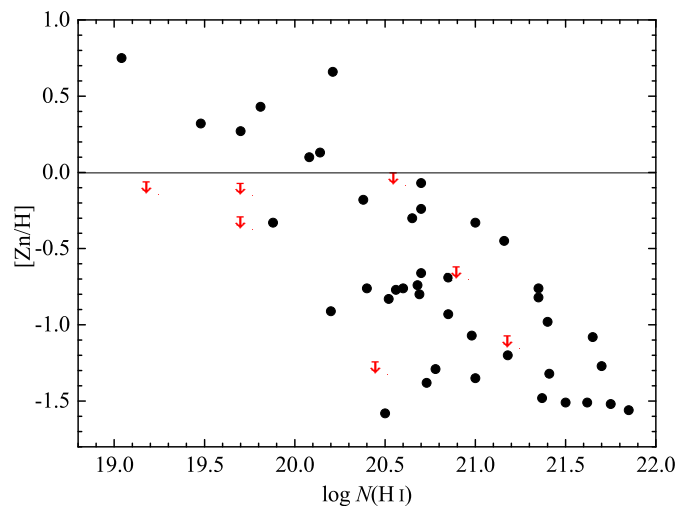


Fig. 10. Metallicity ($[\text{Zn}/\text{H}]$) as a function of neutral gas column density.

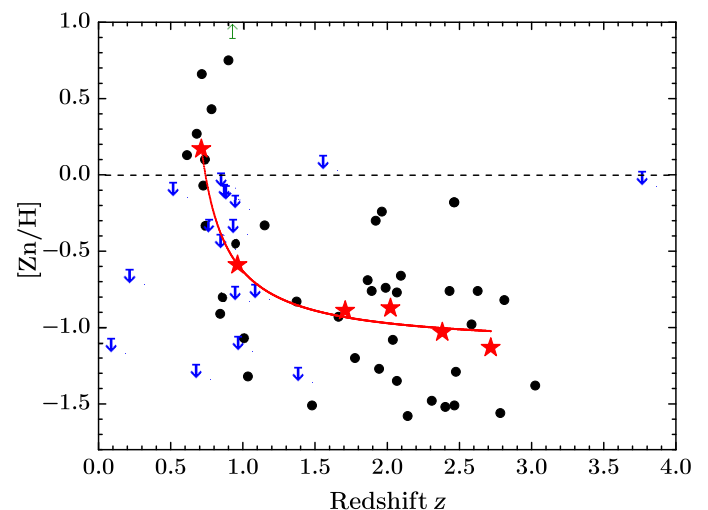


Fig. 11. $[\text{Zn}/\text{H}]$, as an indicator for the metallicity, vs. redshift z . Although as expected the scatter is remarkable, this plot indicates on average higher metallicities for younger systems.

dust depletion not only depends on the overall metallicity of the gas, but also on other physical parameters, such as densities, temperatures and the strengths of the interstellar radiation fields (e.g., Draine (2003)).

Fig. 10 shows a clear trend for decreasing metallicity with increasing H I column density. For DLAs this trend is well-known (e.g., Khare et al. (2007)). Both dependencies put together lead to a weak trend of less severe dust depletion for increasing hydrogen column density.

For Galactic sightlines exactly the opposite trend is observed (Welty & Crowther 2010). This is because the absorbing gas clouds in the Milky Way have similar metallicities and so indeed depletion is more severe for increasing $N(\text{H I})$, because, on average, gas volume densities increase with increasing $N(\text{H I})$ ³. In our sample of extragalactic absorbers, in contrast, we sample multiple arbitrary sightlines

³ In a 5 dimensional phase space with the axes dust depletion $D(X)$, $n(\text{H})$, T , strength of radiation field and metallicity all systems we expect to lay on a 4 dimensional hyper surface.

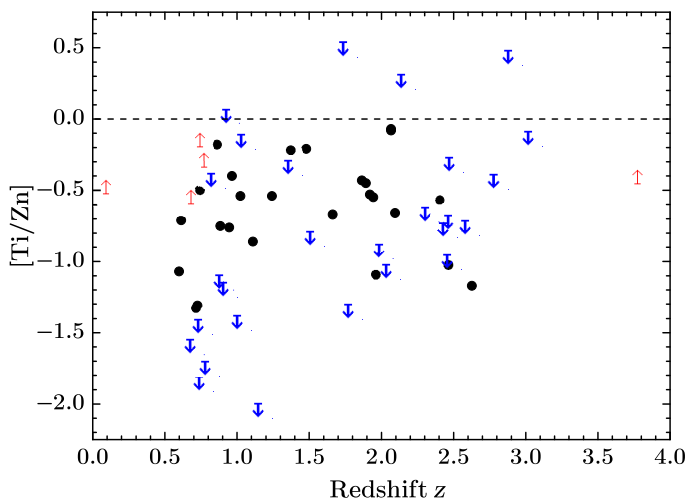


Fig. 12. $[\text{Ti}/\text{Zn}]$ vs. redshift z . In contrast to $[\text{Zn}/\text{H}]$ (Fig. 11), there's no comparable trend visible for $[\text{Ti}/\text{Zn}]$ as a function of z .

through *different* (unrelated) optically thick gas environments and each absorber (i.e., each data point) is characterized by its own metallicity and dust properties (sightline averaged). The distribution of data points for the intervening data points further depends strongly on the cross section of the absorbing gas environments. Obviously, low-metallicity, high-column density neutral gas regions have a larger absorption cross section than high-metallicity environments with somewhat lower neutral gas columns.

Unfortunately, the derived parameters for the class 1 systems include column densities for either H I or Zn II , but not both species together. Only for one class 1 system we know $N(\text{H I})$ and a lower limit for $N(\text{Zn II})$. Table A.1 indicates that class 1 systems are characterized by $[\text{Ti}/\text{Zn}]$ ratios that are larger than -0.8 , while class 2 systems have $[\text{Ti}/\text{Zn}] \leq -0.8$, typically. If we consider the $[\text{Ti}/\text{Zn}]$ ratio as discriminator also for the 57 absorbers without Ca II information in Table A.2, we separate 18 systems with $[\text{Ti}/\text{Zn}] > -0.8$ (sample C) from those 12 systems with $[\text{Ti}/\text{Zn}] \leq -0.8$ (sample D). The 27 systems for which there are only limits on $[\text{Ti}/\text{Zn}]$ that do not allow us to distinguish between sample C and D are collected in sample E.

The mean Zn abundance in sample C absorbers is $\langle [\text{Zn}/\text{H}] \rangle = -0.80 \pm 0.47$, which is mildly lower than the mean Zn abundance in sample D ($\langle [\text{Zn}/\text{H}] \rangle = -0.37 \pm 0.65$, although the uncertainties are substantial). **The only one value for the Zn abundance of a class 1 system is comparatively low ($[\text{Zn}/\text{H}] < -1.08$), while for Class 2 systems it is comparatively high ($\langle [\text{Zn}/\text{H}] \rangle = 0.04$).** Thus, if absorbers in sample A (=class 1) and sample C have similar dust properties (as suggested by the similarly high $[\text{Ti}/\text{Zn}]$ ratios) and both samples belong to class 1 systems, the observed trend is in line with our previous suggestion, namely that class 1 systems typically represent metal- and dust-poor gas environments where the Ti depletion is much less severe than for Ca, so that the observed Ti/Ca ratios are relatively high. Although our data do not confirm metallicity as the only parameter determining the dust depletion, the observed systematic differences

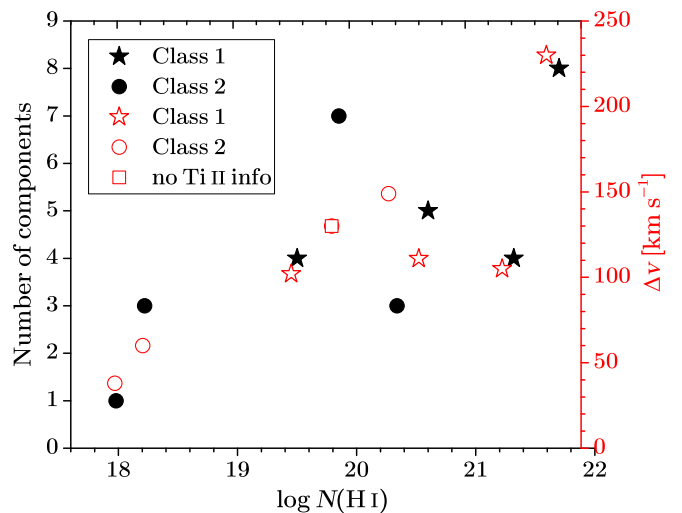


Fig. 13. Number of components and rest frame velocity width Δv of the $\text{Ca II } \lambda 3934$ absorption feature vs. $\log N(\text{H I})$ for class 1 & 2 systems.

in $[\text{Ti}/\text{Zn}]$ demonstrate that both samples (C & D) generally exhibit explicitly different dust properties.

4.2.3. Redshift dependency of abundance and depletion properties

Here we shortly discuss the redshift dependency of the metallicity and titanium dust depletion in our absorber sample. In Fig. 11 we have plotted the Zn abundance in the individual absorbers as a function of z (black filled circles). The distribution of data points exhibits substantial scatter. To explore the global trend we binned every seven systems, calculated the average values of the metallicity ($[\text{Zn}/\text{H}]$) and redshift and fitted a reciprocal function (red stars and red solid line). One can see that, on average, the metallicity decreases with increasing redshift (see also Rafelski et al. (2012)).

While the mean Zn abundance in the absorbers decreases with increasing redshift, Fig. 12 shows that Ti dust depletion (as indicated by the Ti/Zn ratio) has no striking redshift dependence, but instead scatters with ~ 2.5 dex. There is a weak tendency for very low-redshift systems having (on average) a lower Ti/Zn ratio (i.e., a larger Ti depletion), which would be in line with the higher average metallicity of low- z and the presumably higher dust content. This trend becomes significant, if the upper limits for Ti/Zn (blue arrows) are taken into account.

Such a large scatter for Ti/Zn is not surprising because the dust content is not only a function of the global metallicity of the absorbers (which itself exhibits a huge spread; see above), but also depends on other parameters such as local gas density, temperature, and strength of the interstellar radiation field.

4.2.4. The role of absorber kinematics and impact parameters

Fig. 13 shows that for most of the systems for which information on the number of components (N_{comp}), the rest-frame velocity width of the Ca II absorption (Δv), as well as the H I column density is available there is a correlation between these parameters: Δv increases with an increas-

ing component number and both parameters increase for increasing $\log N(\text{H I})$. These trends hold for both, class 1 and class 2 systems. Obviously, the (predominantly neutral) gas phase traced by Ca II is kinematically more complex in high-column density systems than in low-column density absorbers (see also Richter et al. (2011)).

Less clear is the dependence of the parameters N_{comp} , Δv , $\log N(\text{H I})$, $[\text{Ca}/\text{H}]$, and $[\text{Ti}/\text{Ca}]$ on the impact parameters d of the absorbers to their host galaxies (Fig. A.2). Only for a few systems information on d is available, so that we refrain from drawing any conclusions from these plots.

4.2.5. Notes on nucleosynthetic aspects

Out of the three examined elements, Ca, Ti, and Zn, only Ca is a true alpha element, meaning that the most abundant isotope ^{40}Ca , with a natural relative abundance of $\sim 97\%$, is a direct result of the so called alpha-process. Alpha elements or isotopes, respectively, are built up by the addition of α -particles during the last phase of a massive stars life, and their nuclei consist of an integer multiple of an α -particle. Alpha elements mainly are produced during or short before core-collapse supernovae. Although not a direct member of the alpha process, many authors (e.g., Welty & Crowther (2010)) claim an abundance pattern for Ti similar to α elements. On the other hand, zinc and iron trace each other (Timmes, Lauroesch & Truran (1995) and references therein), making Zn an element with an abundance pattern similar as an iron peak element. These elements typically are formed during thermonuclear fusions in Type-1 supernovae.

As a consequence, not only the overall (absolute) metallicities of the examined absorption systems typically are substantially different from the local ISM value, but also the *relative* abundances of Ca, Ti, and Zn may be other than what is indicated by the solar reference values (Asplund et al. 2009). This aspect needs to be kept in mind when interpreting the column densities of the above listed ions in intervening absorption-line systems.

5. Ionization modeling

5.1. Model setup

As mentioned earlier, the ionization potential of Ca II is smaller than that of H I. As a result, in neutral regions the amount of Ca II in the gas phase might be much smaller than the total amount of Ca. To investigate ionization effects for singly-ionized Ca (and for the other two ions, Ti II and Zn II) and their impact on the observed ion ratios in our absorbers we modeled the ionization conditions in the gas using ionization code Cloudy C13.1 (Ferland et al. 2013). Gas absorbers are modeled as plane-parallel slabs of constant neutral columns that are illuminated by an external ionizing radiation field. The big unknown in the modeling setup is the shape and intensity of the UV radiation field that critically determines the ionization balance between Ca II and Ca III in diffuse neutral gas. Cloudy offers several options to pre-define the ionizing radiation field. We here consider two different modeling setups with different radiation fields, which we refer to “halo-model” and “disk-model” in the following. For both models we select the following initial conditions for our Cloudy grids:

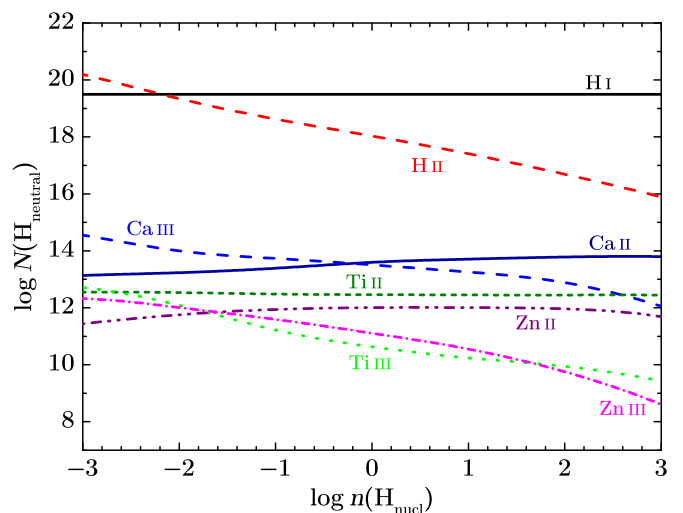


Fig. 14. Example of a Cloudy-model output: logarithm of (ion)-column densities as a function of the log of the hydrogen density for a halo-like system with $\log N(\text{H I}) = 19.5$ and a temperature of 5000 K. The column densities N are given in cm^{-2} , the density n in cm^{-3} .

- Cosmic microwave background at $z = 0.5$,
- Cosmic ray background,
- Gas temperature grid with $T/10^3 \text{ K} \in \{0.1, 0.5, 1, 2.5, 5, 10, 20\}$,
- H I column-density grid with $\log [N(\text{H I})/\text{cm}^{-2}] \in \{19.5, 20.5, 21.5, 22.5\}$,
- Solar reference abundances given by Asplund et al. (2009), and
- Standard ISM-grain properties (`grains ISM command`).

Note that included `grains ISM` option does *not* affect the gas-phase abundances of the elements included in the dust grains, i.e., dust *depletion* effects are not included in the model. **Also note that the true relative abundances may differ from the solar values and also the dust grain composition may be different from the composition assumed via the `grains ISM command`. This may lead to further uncertainties in the assumed model.**

The ionizing radiation field in the disk model is based on the local, unextinguished interstellar Galactic radiation field of Black (1987) (via `table ISM` command). The halo-model, in contrast, assumes the Haardt & Madau (2005) extragalactic UV background field (via the `table HM05` command) normalized at $z = 0.3$. For comparison, the spectral energy distribution of both background fields are shown in Fig. A.1 in the Appendix.

5.2. Modeling results

As an illustration for a typical Cloudy output in Fig. 14 we show the model predictions for the column densities of the relevant ionization states of H, Ca, Ti, and Zn as a function of the gas density for an absorber that is exposed to the extragalactic UV field (halo-model).

For the two model grids (disk model, halo model) we investigate, under which conditions the considered metal ions (singly-ionized Ca, singly-ionized Ti, singly-ionized Zn) represent the dominant ionization states in the gas. In particular, we constrain the critical hydrogen density $\log n_{\text{crit}}$ that

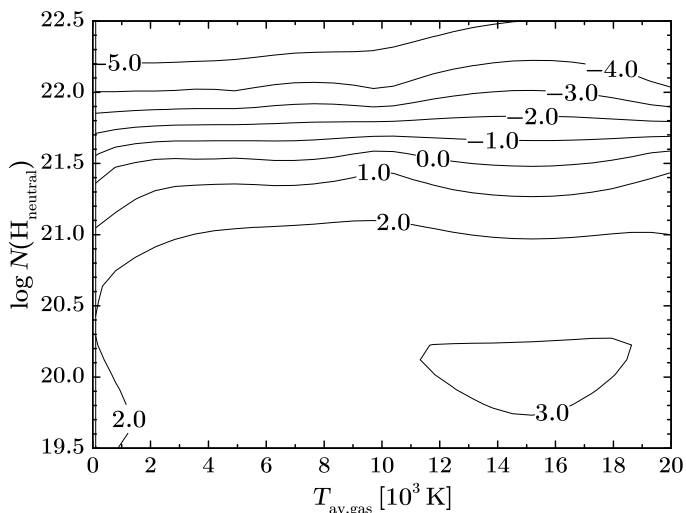


Fig. 15. Cloudy result for the disk model grid: contour plot of the critical hydrogen density $\log n_{\text{crit}}$ above which $N(\text{Ca II}) \geq N(\text{Ca III})$ in the $N(\text{H}_{\text{neutral}})/T$ space.

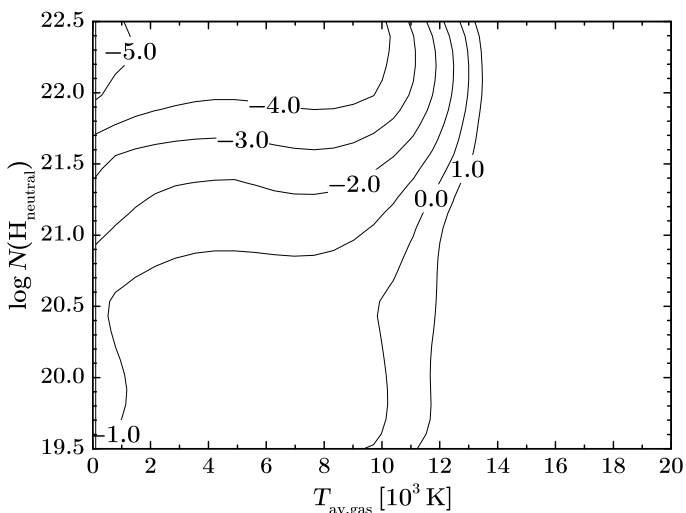


Fig. 16. Cloudy result for the halo model grid: contour plot of the critical hydrogen density $\log n_{\text{crit}}$ above which $N(\text{Ca II}) \geq N(\text{Ca III})$ in the $N(\text{H I})/T$ space. Above 12000 K Cloudy only delivers solutions for which $N(\text{Ca II}) < N(\text{Ca III})$ for all $\log n(\text{H}_{\text{nucl}})$.

separates from each other the dominant ionization states for H, Ca, Ti, and Zn in their characteristic gas phases. In Figs. 15 and 16 we show the resulting values for n_{crit} for Ca II as contours in the $N(\text{H I})/T$ phase space.

The main results from the Cloudy calculation for the two model-grids can be summarized as follows:

Disk model: the critical hydrogen density n_{crit} for which $N(\text{H I}) = N(\text{H II})$ and $N(\text{Ca II}) = N(\text{Ca III})$, respectively, turns out to be independent of the gas temperature. For hydrogen, $\log n_{\text{crit}}$ increases smoothly with decreasing $N(\text{H I})$. For Ca, in contrast, $\log n_{\text{crit}}$ falls steeply for $\log N(\text{H I}) > 21.5$. The disk model indicates that hydrogen is predominantly neutral for all $\log n_{\text{H}} > 0$. Ca II is expected to be the dominant Ca ion for all $\log N(\text{H I}) > 22$, while Ca III is dominant for all $\log N(\text{H I}) < 21.5$. Ti II or Zn II represent the dominant Ti- and Zn-ions, respectively, in

the entire parameter phase space.

Halo model: for gas temperatures above 1.5×10^4 K hydrogen is predominantly ionized, while for temperatures below 1.2×10^4 K hydrogen is predominantly neutral. Only for temperatures below 12×10^3 K and densities $\log n_{\text{H}} > 0$ Ca II is expected to be the dominant ionization state of Ca in these environments, while Ca III dominates for gas that is warmer and/or more diffuse. As for the disk model, Ti II or Zn II are the dominant ions in the entire parameter phase space.

In conclusion, the Cloudy model grids suggest that the interpretation of Ca II column densities and ion ratios that include Ca II in individual absorbers is problematic without knowing the exact local physical conditions. For singly-ionized Ti and Zn, in contrast, the local physical conditions are less important and thus the observed Ti II and Zn II column densities provide robust measures for the gas-phase abundances of these elements in predominantly neutral gas regions.

Despite these theoretical uncertainties for the interpretation of Ca II (either as dominant or non-dominant ion) in individual intervening absorption systems, the *observed* relation between Ca II/H I and H I (Fig. 4) indicates that the analysis of Ca II in a large-enough sample does provide useful information on the dust depletion properties in such systems if compared to other observable ions that co-exist with singly-ionized Ca in the same gas phase.

6. Summary

In this paper we have studied dust depletion of Ti and Ca in gas in and around galaxies by analyzing Ti/Ca abundance ratios in intervening absorption-line systems at low and high redshift.

First, we have investigated high-resolution optical spectra obtained by UVES/VLT and spectroscopically analyzed 34 absorption-line systems at $z_{\text{abs}} \leq 0.5$ to measure column densities (or limits) for Ca II and Ti II. Secondly, We have complemented our UVES data set with previously published absorption-line data on Ti/Ca for redshifts up to $z \approx 3.8$ and created an absorber sample containing more than 100 absorbers including DLAs, sub-DLAs, and LLS.

Our study suggests that there are two distinct populations of Ti/Ca absorbing systems with either high or low Ti/Ca ratios. We refer to these two populations as “class 1” and “class 2” absorbers, respectively,

Class 1 absorbers are characterized by i) relatively high Ti/Ca-ratios ($[\text{Ti}/\text{Ca}] \gtrsim +1.0$), ii) relatively low metallicities ($[\text{Zn}/\text{H}] \lesssim -1.0$), iii) and relatively mild Ti-dust-depletion values ($[\text{Ti}/\text{Zn}] > -0.8$). In class 1 absorbers, Ti/Ca appears to increase with increasing $N(\text{H I})$, implying that dust depletion becomes progressively more important for Ca compared to Ti in systems with large neutral gas columns. The simultaneous significant detection of both ions, Ca II & Ti II, is a good indicator for observing a class 1 system. Class 1 systems obviously represent metal-poor gas absorbers with relatively low dust content.

In contrast to class 1 systems, class 2 absorbers typically have higher metallicities ($[\text{Zn}/\text{H}] \gtrsim 0.0$) and a higher dust-to-gas ratio. Here, the Ti depletion reaches similar values as for Ca, leading to systematically lower Ti/Ca-ratios ($[\text{Ti}/\text{Ca}] \lesssim +1.0$). The class 2 systems do not show any systematic relation between H I column density and the ion ratios $[\text{Ti}/\text{H}]$ and $[\text{Ti}/\text{Ca}]$.

From our `Cloudy` ionization model grids we conclude that Ti II & Zn II are the dominant ionization states of Ti & Zn in neutral gas within a broad range of physical conditions. For Ca, however, the `Cloudy` models predict a strong dependency of the ionization fraction of singly- and double-ionized Ca on the local physical conditions. Therefore, ionization effects and dust depletion effects are difficult to disentangle for Ca II in individual absorbers without information on other depleted and undepleted species.

The Ti/Ca ratios in class 1 systems are very similar to those observed in the LMC and SMC, but are substantially higher than what is found in the Milky Way ISM. This trend is in line with the above stated conclusion that class 1 systems with high Ti/Ca ratios trace dust- and metal-deficient gas environments in and around galaxies.

Our study suggests that the Ti/Ca ratio in intervening absorption systems may be used as indicator for the metal- and dust-content of intervening absorbers. This might be of relevance in particular for those low-redshift systems for which direct information on the metallicity cannot be obtained due to the lack of UV spectral data that would give access to the Lyman series of H I. In addition, future studies on Ti/Ca in intervening absorbers *in combination* with supplementary data on galaxy impact parameters for a large-enough absorber/galaxy sample hold the prospect to boost our understanding of the distribution of dust in the inner and outer regions of galaxies.

References

- Asplund M., Grevesse N., Sauval A.J. & Scott P., 2009, arxiv.org/pdf/astro-ph/0909.0948.pdf
- Black J.H., 1987, In D.J. Hollenback and H.A. Thronson, Jr., editors, *Interstellar Processes*, vol. 134 of *Astrophysics and Space Science Library*, pages 731-744
- Chen H.-W., Kennicutt R.C. & Rauch M., 2005, *ApJ*, 620, 703
- Draine .T., 2003, *Ann. Rev. Astron. Astrophys.*, 41:241-89
- Ferland G.J., Porter R.L., van Hoof P.A.M., Williams R.J.R., Abel N.P., Lykins M.L., Shaw G., Henney W.J. & Stancil P.C., 2013, the 2013 Release of `Cloudy`. *Revista Mexicana de Astronomia y Astrofisica*, 49:137-163
- Hunter I., Smoker J. V., Keenan F. P., Ledoux C., Jehin E., Cabanac R., Melo C., & Bagnulo S., 2006, *MNRAS*, 367, 1478
- Jenkins E.B., Bowen D.V., Tripp T.M., Sembach K.R., Leighly K.M., Halpern J.P. & Lauroesch J.T., 2003, *ApJ*, 125, 2824
- Jenkins E.B., 2009, *ApJ*, 700, 1299
- Khare P., Kulkarni V.P., Péroux C., York D.G., Laroesch J.T. & Meiring J.D., 2007, *A&A*, 464, 487
- Lane W., Smette A., Briggs F., Rao S., Turnshek D. & Meylan G., 1998, *AJ*, 116, 26
- Le Brun V., Bergeron J., Boisse P. & Deharveng J.M., 1997, *A&A*, 321, 733
- Miller E.D., Knezek P.M. & Bregman J., 1999, *ApJ*, 510, L95
- Morton D.C., 2003, *ApJS*, 149, 205
- Planck Collaboration (for details see article), 2013, *A&A*, 571, A16
- Prochaska J.X., Herbert-Fort S. & Wolfe A.M., 2005, *ApJ*, 635, 123
- Rafelski M., Wolfe A.M., Prochaska J.X., Neeleman M. & Mendez A.J., 2012, *ApJ*, 755, 89
- Rao S.M., Nestor D.B., Turnshek D.A., Lane W.M., Monier E.M. & Bergeron J., 2003, *ApJ*, 595, 94
- Richter P., Savage B.D., Wakker B.P., Sembach K.R. & Kalberla P.M.W., 2001, *ApJ*, 549, 281
- Richter P., Krause F., Fechner C., Charlton J.C. & Murphy M.T., 2011, *A&A*, 528, A12
- Ryabinkov A.I., Kaminker A.D., Varshalovich D.A., 2004, *A&A*, 412, 707-709
- Savage B.D. & Sembach K.R., 1996, *Annu. Rev. Astron. Astrophys.*, 34:279-329
- Timmes F.X., Lauroesch J.T. & Truran J.W., 1995, arxiv.org/pdf/astro-ph/9504031.pdf
- Tumlinson J., Shull J.M. & Rachford B.L., 2002, *ApJ*, 566, 857
- Turnshek D.A., Rao S.M., 2002, *ApJ*, 572, L10
- Vladilo G., Centurión M., Falomo R. & Molaro P., 1997, *A&A*, 327, 47
- Wakker B.P. & Mathis J.S., 2000, *ApJ*, 544, L107
- Wasson J.T., 1985, *Meteorites: Their Record of the Early Solar System History*. Freeman, New York
- Welty D.E. & Crowther P.A., 2010, *MNRAS*, 404, 1321

Appendix A: Additional Figures and Tables

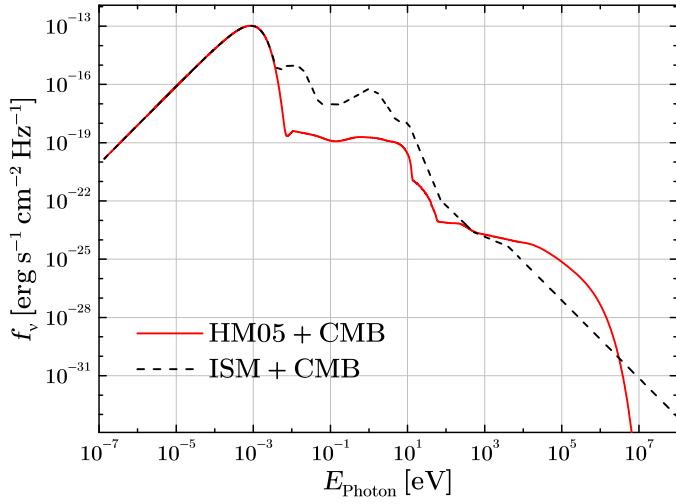


Fig. A.1. Background radiation fields as described in the text.

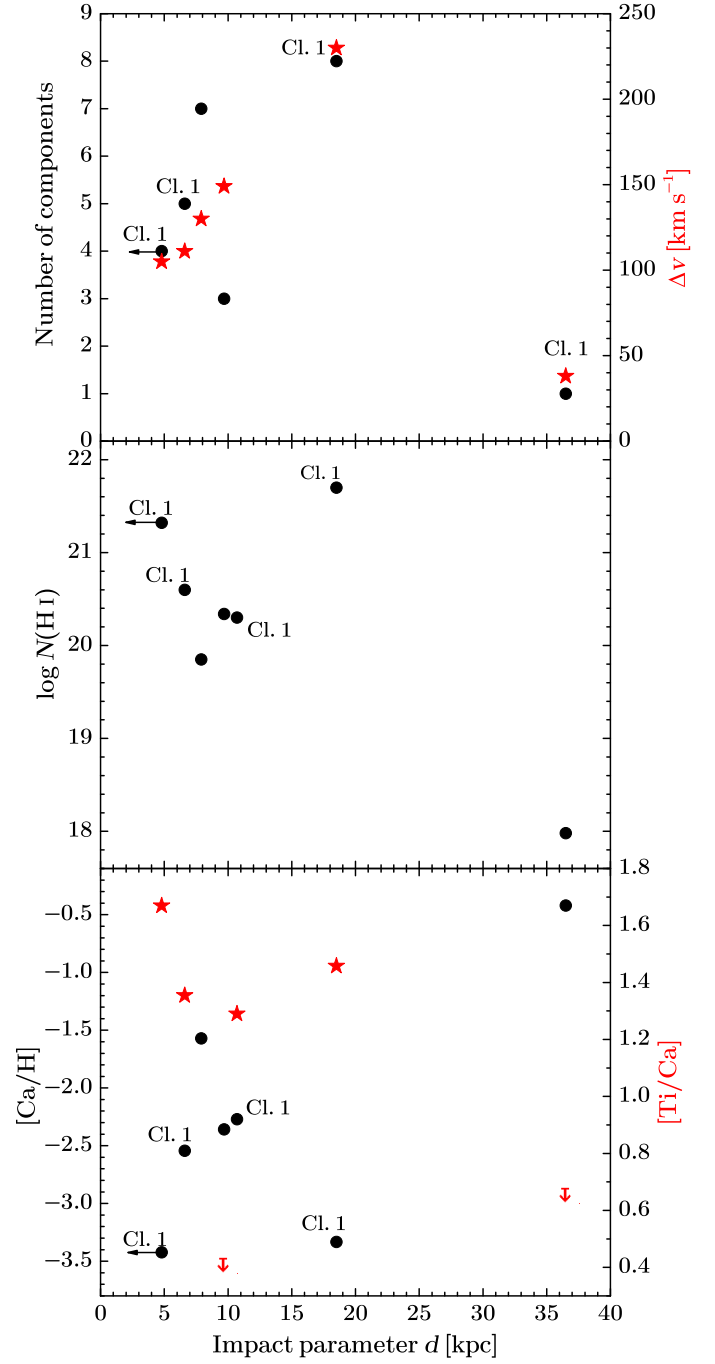


Fig. A.2. Relations between N_{comp} , the number of components, $\log N(\text{H I})$, rest frame velocity width Δv of the $\text{Ca II } \lambda 3934$ absorption feature, ratios $[\text{Ca}/\text{H}]$, $[\text{Ti}/\text{Ca}]$ and the impact parameter d . Class 1 systems are labeled with “Cl. 1”.

Table A.1. Data for Ca II systems with known Ti II column density (SAMPLE A) or upper limits for Ti II (SAMPLE B). A star symbol in front of the sightline marks systems analyzed in this paper. Data of all other systems are from table A3 in Welty & Crowther (2010). With one exception all sample A systems are also class 1 systems ($[\text{Ti}/\text{Ca}] \gtrsim +1$). The sample A system with $z = 1.0232$ is a class 2 system ($[\text{Ti}/\text{Ca}] \approx 0$). For most of the sample B systems the upper limit of $[\text{Ti}/\text{Ca}]$ is too high to decide whether it is a class 1 or 2 system. We expect systems with $[\text{Ti}/\text{Ca}] < 0.5$ to be class 2 systems.

Class	QSO / sightline	z_{abs}	$\log N(\text{H I})$	$\log N(\text{Ca II})$	$\log N(\text{Ti II})$	$\log N(\text{Zn II})$	[Ca/H]	[Ca/Zn]	[Ti/H]	[Ti/Zn]	[Ti/Ca]	[Zn/H]
SAMPLE A: Ca II systems with known Ti II column density												
1	Q0738+313	0.0912	21.18	12.32	12.53	< 12.66	-3.2	>	-1.6	>	-0.52	1.6
1	*J095456+174331	0.23782	21.32 ± 0.07 ^a	12.21 ± 0.023	12.565 ± 0.046	-3.45 ± 0.14	-	-1.71 ± 0.17	-	-	1.74 ± 0.16	< -1.08
1	*J235731-112539	0.24763		12.849 ± 0.033	12.917 ± 0.067	-	-	-	-	-	1.46 ± 0.19	-
1	*J113007-144927	0.31273	21.71 ± 0.09 ^b	12.7142 ± 0.0062	12.782 ± 0.021	-3.33 ± 0.14	-	-1.88 ± 0.16	-	-	1.46 ± 0.12	-
1	*J123200-022404	0.39498	20.6 ^c	12.398 ± 0.014	12.363 ± 0.040	-2.542	-	-1.187	-	-	1.36 ± 0.15	-
1	*J045608-215909	0.47439	19.5 ^d	12.23 ± 0.014	11.825 ± 0.046	-1.61	-	-0.625	-	-	0.99 ± 0.15	-
1	Q0118-272	0.558	20.3 ^e	12.37	12.27	-2.27	-	-0.98	-	-	1.29	-
1	J0846+0529	0.7429		13.06	13.00	< 12.8	>	-1.52	>	-0.19	1.33	-
1	J1007+2853	0.8839		13.33	13.13	13.49	-	-1.94	-	-0.75	1.19	-
1	J1129+0204	0.9650		13.11	12.79	12.8	-	-1.47	-	-0.4	1.07	-
2	J0953+0801	1.0232		13.57	12.10	12.25	-	-0.46	-	-0.54	-0.08	-
1	J1430+0149	1.2418		12.85	12.79	12.94	-	-1.87	-	-0.54	1.33	-
SAMPLE B: Ca II systems with upper limits for the Ti II column density												
2	*J121509+330955	0.00396	20.34 ^f	12.366 ± 0.018	< 11.361	-2.314	-	< -1.93	-	-	< 0.39	-
2	*J133007-205616	0.01831		13.049 ± 0.025	< 11.817	-	-	< 0.26	-	-	< 0.16	-
?	*J215501+092224	0.08091	17.98 ^g	11.861 ± 0.047	< 11.182	-0.46	-	< -2.37	-	-	< 0.72	-
?	Q0738+313	0.2210	20.90	11.91	< 11.480	-3.33	>	-2.7	-	-	< 0.96	< -0.63
?	*J012517-001828	0.23864		11.447 ± 0.092	< 11.298	-	-	-	-	-	< 1.24	-
2	*J000344-232355	0.27051		11.660 ± 0.025	< 10.827	-	-	-	-	-	< 0.56	-
?	*J142249-272756	0.27563		12.135 ± 0.012	< 11.392	-	-	-	-	-	< 0.65	-
?	*J042707-130253	0.28929		11.626 ± 0.061	< 11.378	-	-	-	-	-	< 1.15	-
?	*J102837-010027	0.32427		12.496 ± 0.029	< 11.679	-	-	-	-	-	< 0.58	-
?	*J231359-370446	0.33980		12.542 ± 0.030	< 12.190	-	-	-	-	-	< 1.04	-
?	*J142253-000149	0.34468		12.535 ± 0.046	< 11.872	-	-	-	-	-	< 0.73	-
?	*J110325-264515	0.35896		11.251 ± 0.039	< 10.541	-	-	-	-	-	< 0.68	-
?	*J121140+103002	0.39293		11.388 ± 0.108	< 11.208	-	-	-	-	-	< 1.21	-
?	*J050112-015914	0.40310		12.350 ± 0.048	< 12.075	-	-	-	-	-	< 1.12	-
2	*J224752-123719	0.40968		12.268 ± 0.037	< 11.337	-	-	-	-	-	< 0.46	-
?	*J232820+002238	0.41277		11.521 ± 0.073	< 11.138	-	-	-	-	-	< 1.01	-
?	*J051707-441055	0.42913		10.476 ± 0.059	< 10.192	-	-	-	-	-	< 1.11	-
?	*J220743-534633	0.43720		12.002 ± 0.069	< 11.498	-	-	-	-	-	< 0.89	-
?	*J044117-431343	0.44075	18.22 ± 0.20 ^h	11.482 ± 0.061	< 11.197	-1.01 ± 0.30	-	< 0.026	-	-	< 1.11	-
?	*J144653+011356	0.44402		11.338 ± 0.110	< 10.864	-	-	-	-	-	< 0.92	-
?	*J124646-254749	0.49282		12.773 ± 0.079	< 11.922	-	-	-	-	-	< 0.54	-
2	Q2335+1501	0.6798	19.70	12.41	< 11.36	-1.63	-1.9	< -1.29	< -1.56	-	< 0.34	0.27
2	Q1436-0051	0.7377	20.08	12.83	< 11.71	12.74	-1.59	< -1.32	< -1.42	< -1.42	< 0.27	0.1
?	J1203+1028	0.7463		13.05	< 11.20	12.63	-1.36	< -1.82	< -1.82	< -1.82	< -0.46	-
?	Q1009-0026	0.8866	19.48	12.26	< 11.64	12.36	-1.56	< -0.79	< -1.11	< -1.11	< 0.77	0.32
?	Q1631+1156	0.9004	19.70	12.17	< 11.66	< 12.18	-1.87	< -0.99	< -0.99	< -0.99	< 0.88	< -0.08
?	Q0826-2230	0.9110	19.04	11.75	< 11.58	12.35	-1.63	< -0.41	< -0.41	< -0.41	< 1.22	0.75
?	Q1436-0051	0.9281	< 18.80	12.28	< 12.71	>	-0.86	>	>	>	< 1.82	> 0.90
?	J0517-441	1.1496		12.74	< 10.6	12.22	-1.26	< -2.01	< -2.01	< -2.01	< -0.75	-
2	HE0515-4414	1.151	19.88	12.72	< 11.7	12.11	-1.5	< -1.13	< -0.80	< -0.80	< 0.37	-0.33

References. (a) Rao et al. (2003); (b) Lane et al. (1998); (c) Le Brun et al. (1996); (d) Turnshek & Rao (2002); (e) Vladilo et al. (1997); (f) Miller et al. (1999); (g) Jenkins et al. (2003); (h) Value calculated using the observed equivalent width of the $\text{H}\alpha$ line given by Ryabinkov et al. (2004) (1.53(11) Å) with the assumption that this line is in the damping part of the curve of growth.

Table A.2. Data for Ti II systems or upper limit Ti II systems without any Ca II information. Redshifts and column densities are taken from Welty & Crowther (2010; see references therein). For calculation of ratios solar abundances given by Asplund et al. (2009) are assumed.

QSO	z_{abs}	$\log N(\text{H I})$	$\log N(\text{Ti II})$	$\log N(\text{Zn II})$	[Ti/H]	[Ti/Zn]	[Zn/H]
SAMPLE C: [Ti/Ca] > -0.8							
Q0058+019	0.612	20.14	12.51	12.83	-0.58	-0.71	0.13
Q1122-168	0.682	20.45	11.56	< 11.76	-1.84	> -0.59	< -1.25
J1107+0048	0.7403	21.00	13.12	13.23	-0.83	-0.50	-0.33
Q0153+0009	0.7714	19.70	12.02	< 11.96	-0.63	> -0.33	< -0.3
Q0454+039	0.8598	20.69	12.66	12.45	-0.98	-0.18	-0.80
J1727+5302	0.9449	21.16	12.90	13.27	-1.21	-0.76	-0.45
Q0935+417	1.3726	20.52	12.42	12.25	-1.05	-0.22	-0.83
Q0933+733	1.4790	21.62	12.85	12.67	-1.72	-0.21	-1.51
Q1104-181	1.662	20.85	12.20	12.48	-1.60	-0.67	-0.93
Q2230+025	1.8644	20.85	12.68	12.72	-1.12	-0.43	-0.69
Q1210+17	1.8918	20.60	12.34	12.40	-1.21	-0.45	-0.76
Q2206-199	1.920	20.65	12.77	12.91	-0.83	-0.53	-0.30
Q1157+014	1.944	21.70	12.83	12.99	-1.82	-0.55	-1.27
Q2231-002	2.0661	20.56	12.66	12.35	-0.85	-0.08	-0.77
F0812+32	2.0668	21.00	12.53	12.21	-1.42	-0.07	-1.35
Q2359-02	2.0951	20.70	12.33	12.60	-1.32	-0.66	-0.66
Q0027-1836	2.402	21.75	12.61	12.79	-2.09	-0.57	-1.52
P0133+0400	3.7736	20.55	13.04	< 13.1	-0.46	> -0.45	< -0.01
SAMPLE D: [Ti/Ca] ≤ 0.8							
J0334-0711	0.5976	—	11.9	12.58	—	-1.07	—
J1323-0021	0.716	20.21	12.49	13.43	-0.67	-1.33	0.66
J0256+0110	0.725	20.70	12.27	13.19	-1.38	-1.31	-0.07
Q0138-0005	0.7821	19.81	< 11.48	12.8	< -1.28	< -1.71	0.43
Q0449-1645	1.0072	20.98	< 11.47	12.47	< -2.46	< -1.39	-1.07
Q0014+813	1.11	—	12.36	12.83	—	-0.86	—
Q1331+170	1.7765	21.18	< 11.62	12.54	< -2.51	< -1.31	-1.2
Q0551-364	1.962	20.70	12.32	13.02	-1.33	-1.09	-0.24
Q2318-1107	1.989	20.68	< 12.00	12.50	< -1.63	< -0.89	-0.74
Q0458-020	2.0395	21.65	< 12.49	13.13	< -2.11	< -1.03	-1.08
Q0201+365	2.4628	20.38	< 12.19	12.76	< -1.14	< -0.96	-0.18
Q0836+113	2.4651	20.58	< 12.54	< 12.12	< -0.99	-1.02	-0.18
SAMPLE E: no information about [Ti/Ca] or upper limit too high							
Q2128-123	0.430	19.37	< 11.13	—	< -1.19	—	—
Q0827+243	0.5247	20.30	< 11.76	< 12.8	< -1.49	—	< -0.06
Q1622+238	0.656	20.36	12.35	—	-0.96	—	—
Q2206-199	0.752	—	12.20	—	—	—	—
Q1009-0026	0.8426	20.20	11.85	< 11.85	< -1.30	< -0.39	-0.91
Q0005+0524	0.8514	19.08	< 11.03	< 11.24	< -1.00	—	< -0.4
Q1330-2056	0.8526	19.40	< 11.45	< 11.96	< -0.90	—	< 0.00
Q1228+1018	0.9376	19.41	< 11.65	< 11.67	< -0.71	—	< -0.30
Q1054-0020	0.9514	19.28	< 12.36	< 11.70	< 0.13	—	< -0.14
Q1107+0003	0.9547	20.26	< 13.01	< 12.08	< -0.20	—	< -0.74
Q1220-0040	0.9746	20.20	< 12.47	< 11.69	< -0.68	—	< -1.07
Q1455-0045	1.0929	20.08	< 12.44	< 11.91	< -0.59	—	< -0.73
Q0453-423	1.150	—	< 13.11	< 12.63	—	—	—
J2240-0053	1.3606	—	< 12.71	12.62	—	< -0.30	—
Q0012-0122	1.3862	20.26	< 11.96	< 11.55	< -1.25	—	< -1.27
Q0427-1302	1.5623	18.90	< 12.47	< 11.58	< 0.62	—	< 0.12
Q1946+766	1.7382	—	< 12.45	11.53	—	< 0.53	—
Q0149+33	2.1408	20.50	< 12.17	11.48	< -1.28	< 0.30	-1.58
Q0100+130	2.309	21.37	< 12.21	12.45	< -2.11	< -0.63	-1.48
Q2343+123	2.4313	20.40	< 11.85	12.20	< -1.5	< -0.74	-0.76
Q1223+175	2.4661	21.50	< 12.25	12.55	< -2.20	< -0.69	-1.51
Q0841+129	2.4762	20.78	< 12.16	12.05	< -1.57	< -0.28	-1.29
Q1209+0919	2.5841	21.40	< 12.65	12.98	< -1.70	< -0.72	-0.98
P1253-0228	2.7828	21.85	< 12.84	12.85	< -1.96	< -0.40	-1.56
Q0528-251	2.8110	21.35	< 13.95	13.09	< -0.35	< 0.47	-0.82
Q0347-382	3.0247	20.73	< 12.20	11.91	< -1.48	< -0.10	-1.38
J0255+00	3.2529	20.70	< 12.81	—	< -0.84	—	—

Table A.3. Data for systems with only upper limits for both, Ca II AND Ti II, and data for systems with information only for one ion or systems not matching one of the conditions mentioned before. For no one of the listed systems the values [Ca/Zn], [Ti/Zn] and [Ti/Ca] are calculable. A star symbol in front of the sightline marks systems analyzed in this paper.

QSO	z_{abs}	$\log N(\text{H I})$	$\log N(\text{Ca II})$	$\log N(\text{Ti II})$	$\log N(\text{Zn II})$	[Ca/H]	[Ti/H]	[Zn/H]
Systems with only upper limits both, for Ca II AND Ti II								
Q0827+243	0.2590	–	< 11.60	< 11.96	–	–	–	–
*J162439+234512	0.31759	–	< 11.551	< 11.481	–	–	–	–
*J005102–252846	0.34393	–	< 11.293	< 12.057	–	–	–	–
*J055158–211949	0.43982	–	< 11.875	< 11.584	–	–	–	–
*J030844–295702	0.441	–	< 11.417	< 11.365	–	–	–	–
*J000344–232355	0.45241	–	< 10.466	< 10.635	–	–	–	–
*J014125–092843	0.50053	–	< 10.961	< 11.309	–	–	–	–
Q2352–0028	0.8730	19.18	< 11.01	< 11.36	< 11.67	< –2.51	< –0.77	< –0.07
Systems without any information about Ti II and other systems								
*J044117–431343	0.10114	19.85 ± 0.10^a	12.606 ± 0.013	ood	–	-1.57 ± 0.16	–	–
*J104733+052454	0.31822	–	< 10.853	ood	–	–	–	–
*J094253–110426	0.39098	–	11.929 ± 0.019	blended	–	–	–	–

References. (a) Chen, Kennicutt & Rauch (2004)

Table A.4. Data relating the absorption structure complexity and the absorber galaxy connection. Redshifts, component number and velocity widths of the Ca II $\lambda 3934$ are from Richter et al. (2011). The last column includes the references for impact parameters (calculated from angles using Λ CDM cosmology and the cosmological parameters from Planck Collaboration (2014) listed in Section 2.2.

QSO sightline	z_{abs}	Comp. nr.	$\Delta v_{\text{Ca II } \lambda 3934}$ [km s ^{–1}]	Imp. par. d [kpc]	Ref.
Sample A / Class 1					
J095456+174331	0.23782	4	105	< 4.8	a
J235731–112539	0.24763	3	53	–	–
J113007–144927	0.31273	8	230	18.5	b
J123200–022404	0.39498	5	111	6.6	c
J045608–215909	0.47439	4	102	–	–
Q0118-272	0.558	–	–	10.7	d
Sample B					
J121509+330955	0.00396	3	149	9.7	e
J133007–205616	0.01831	9	378	–	–
J215501+092224	0.08091	1	38	36.5	f
J012517–001828	0.23864	1	22	–	–
J000344–232355	0.27051	2	42	–	–
J142249–272756	0.27563	1	29	–	–
J042707–130253	0.28929	2	122	–	–
J102837–010027	0.32427	2	143	–	–
J110325–264515	0.35896	1	31	–	–
J121140+103002	0.39293	1	30	–	–
J050112–015914	0.40310	3	103	–	–
J224752–123719	0.40968	2	101	–	–
J220743–534633	0.43720	1	26	–	–
J044117–431343	0.44075	3	60	–	–
J144653+011356	0.44402	1	42	–	–
Other systems					
J044117–431343	0.10114	7	130	7.9	g
J231359–370446	0.33980	3	41	–	–
J094253–110426	0.39098	2	31	–	–

References. (a) Rao et al. (2003); (b) Lane et al. (1998); (c) Le Brun et al. (1996); Vladilo et al. (1997); (e) Miller et al. (1999); (f) Jenkins et al. (2003); (g) Chen, Kennicutt & Rauch (2004)